Tensile or compressive plastic deformation of cylinders assisted by cyclic torsion

Z. Mróz [a,*], K. Kowalczyk-Gajewska [a], J. Maciejewski [a], R. B. Pęcherski [a,b],

[a] *Institute of Fundamental Technological Research PAS, Świętokrzyska 21, 00 049 Warsaw, Poland*

[b] *Institute of Structural Mechanics, Faculty of Civil Engineering, Cracow University of Technology, Warszawska 24, 31-155 Cracow, Poland*

Abstract

Technological metal forming processes of extrusion, forging and rolling with imposed cyclic torsion or shear deformation have been recently studied in view of their advantages with respect to monotonic loading processes, cf. Bochniak and Korbel [2-4]. The present work is aimed to analyze such process in the case of simple tension or compression of a cylindrical tube with imposed cyclic torsional deformation. The material element response is assumed as rigid-perfectly plastic or elastic-perfectly plastic. For these models, the analytical solutions can be provided for the steady cyclic responses and the effect of two process parameters, namely the ratio of shear and axial strain rates η and the amplitude of shear strain γ_m, can be clearly demonstrated. Three different regimes of cyclic response can be visualized in the plane η, γ_m. The cyclic response of a cylinder under combined axial compression and cyclic torsion is predicted by considering a simplified model of a set of concentric tubes and neglecting their radial stress interaction. The axial force and torsional moment are then specified by averaging responses of consecutive tubes. The cyclic response diagrams for the cylinder are next generated in terms of axial force and torsional moment related to axial deformation and angle of twist.

1 Introduction

In recent years there has been a growing interest in metal forming processes assisted by cyclic loading. The so called KOBO-type forming proposed by Kor-

* Corresponding author, fax: +4822 8269815

Email addresses: zmroz@ippt.gov.pl (Z. Mróz), kkowalcz@ippt.gov.pl (K. Kowalczyk-Gajewska), jmaciej@ippt.gov.pl (J. Maciejewski), rpecher@ippt.gov.pl (R. B. Pęcherski).

Preprint submitted to Archives of Mechanics

bel and Bochniak [2–4, 10] and applied to extrusion of tubes and wires has demonstrated essential advantages with respect to classical forming processes. The significant reduction of required load for forming, growth of ductility, possible reduction of dissipated energy of forming and finer grain structure are the main beneficial factors cf. also Kong et al [8, 9].

At the micro-mechanical scale, it is observed that destabilization of the developed dislocation substructure occurs with subsequent generation of coarse slip bands propagating in a transgranular mode, thus reducing the stress level required for progressive deformation. Such effects of instabilities of hardened states at large plastic deformation were discussed already by Basinski and Jackson [1, 6]. Also Coffin [7] noted in his work that imposed cyclic deformation could be applied to facilitate the progressive metal forming process.

The present work is aimed at the study of such cyclic deformation assisted process by applying simple constitutive models of plastic response of metals. Our objective is to provide an analytical solution of the steady cyclic deformation process and discuss the effect of two basic parameters η and γ_m representing the ratio of shear and axial strain rates, and the shear strain amplitude. The analysis will be carried out for a perfectly plastic material model satisfying the Huber-Mises yield condition. The types of steady cyclic responses are presented by the interaction diagrams in the plane γ_m, η. Both piecewise linear and harmonic shear strain controls are considered. The plastic dissipation in axial and torsional straining is presented and referred to the dissipation in the monotonic tension or compression process.

The study will be pertained to a circular cylinder or tube axially deforming with a specified rate and subjected to alternative twist with specified rate and amplitude. Most cyclic loading experiments available in literature have been performed at specified axial stress values in order to study ratchetting strain induced by cyclic torsion, cf. Mróz and Rodzik [11]. Here, we shall refer to tests performed by Bochniak and Korbel [2] and Grosman [5] for the case of tension or compression of cylindrical specimens with imposed cyclic torsion. The analysis will be presented first for a case of cylindrical tube and next the response of a cylinder will be predicted by superposing solutions for a set of tubes of decreasing radii. The analysis with account for material hardening and recovery effects will be presented in a separate paper.

2 Problem formulation for a thin-walled tube.

Consider a thin walled tube of initial radius r_0, and length l_0 and wall thickness t_0 subjected to axial tension or compression. Assume the axial strain rate to be specified and constant. The alternating torsion is imposed in order to reduce the axial stress and applied axial force in order to execute the process. Denote by ε_x and γ_{xy} the axial and shear strain components and their rates by $\dot{\varepsilon}_x$, $\dot{\gamma}_{xy}$. The Cauchy stress components referred to the actual configuration are σ_x, τ_{xy}. For simplicity, consider first the small strain formulation which can next be improved

by considering configuration changes for large compressive or tensile strains. The deformation program is shown in Fig. 1.

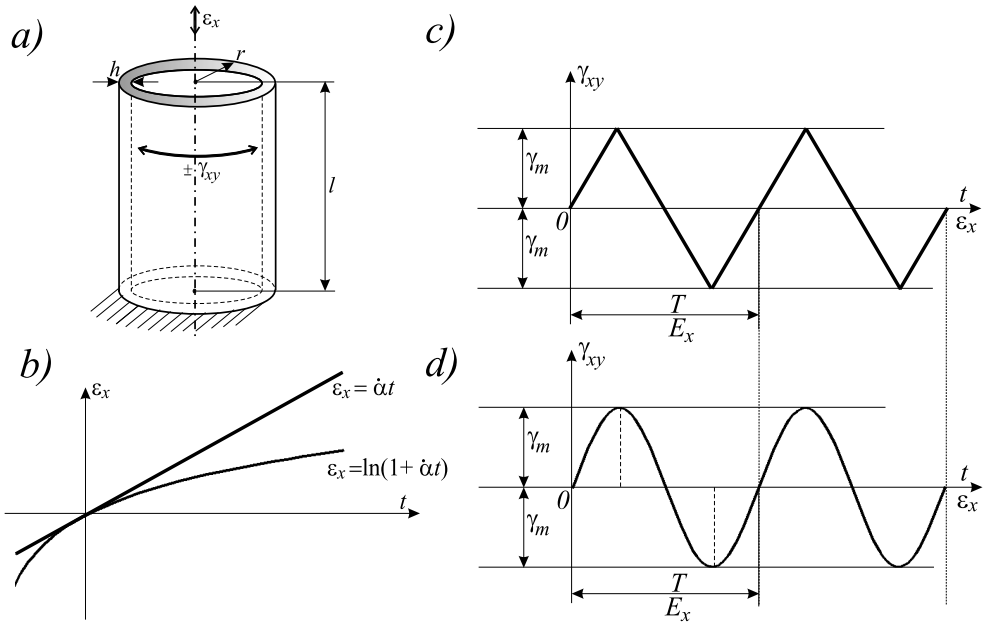

Figure 1. Axial and torsional deformation program: a/ tube dimensions, b/ longitudinal strain $\varepsilon_x(t)$, c/ piecewise linear variation of shear strain, d/ harmonic variation of shear strain $\gamma_{xy}(t)$.

For uniform in time length variation ($l = l_0(1 \pm \dot{\alpha}t)$) the axial strain and strain rate are $|\varepsilon_x| = \dot{\alpha}t$, $|\dot{\varepsilon}_x| = \dot{\alpha}$, where $\dot{\alpha} = |\dot{l}|/l_0$. For the logarithmic strain measure there is $\varepsilon_x = \ln(1 \pm \dot{\alpha}t)$ and $|\dot{\varepsilon}_x| = |\dot{l}|/l = \pm\dot{\alpha}l/(1 \pm \dot{\alpha}t)$. The shear strain is assumed to oscillate with the amplitude $2\gamma_m$ and the period T. For piecewise linear oscillation, Fig. 1c, we have $\dot{\beta} = \dot{\gamma}_{xy} = 4\gamma_m/T$. Denote the ratio of rates of shear and axial strains by η, thus

$$\eta = \frac{\dot{\beta}}{\dot{\alpha}} = const, \quad \dot{\beta} = \frac{4\gamma_m}{T}, \quad \dot{\beta} > 0, \quad \dot{\alpha} > 0. \tag{2.1}$$

For the harmonic variation of γ_{xy}, Fig. 1d, we can write

$$\gamma_{xy} = \gamma_m \sin\left(\frac{2\pi}{T}t\right), \quad \dot{\gamma}_{xy} = \frac{\pi}{2}\dot{\beta}\cos\left(\frac{2\pi}{T}t\right), \quad \dot{\beta} = \frac{4\gamma_m}{T}$$

and the ratio of strain rates is

$$\frac{\dot{\gamma}_{xy}(t)}{|\dot{\varepsilon}_x|} = \eta\frac{\pi}{2}\cos\left(\frac{2\pi}{T}t\right) = \eta\frac{\pi}{2}\cos\left(\frac{2\pi}{T}\frac{|\varepsilon_x|}{\dot{\alpha}}\right) = \eta\frac{\pi}{2}\cos\left(2\pi\frac{|\varepsilon_x|}{E_x}\right), \tag{2.2}$$

where $E_x = \frac{4\gamma_m}{\eta}$ is the strain period corresponding to time period T. Let us note that the time measure can be replaced by the axial strain $|\varepsilon_x| = \dot{\alpha}t$.

3 Deformation analysis for a rigid perfectly plastic material model

To understand the constitutive model assumptions in the analysis of cyclic response of tube, we provide first the analytical solution for the perfectly plastic material model assuming the Huber-Mises yield condition and the associated flow rule. The constitutive equations can be written in the form:

- yield condition

$$F = \sqrt{\sigma_x^2 + 3\tau_{xy}^2} - \sigma_0 \leq 0, \tag{3.1}$$

- rate equations

$$\begin{aligned} \dot{\varepsilon}_x &= \dot{\varepsilon}_x^e + \dot{\varepsilon}_x^p = \frac{\dot{\sigma}_x}{E} + \dot{\lambda}\frac{\sigma_x}{\sigma_0}, \\ \dot{\gamma}_{xy} &= \dot{\gamma}_{xy}^e + \dot{\gamma}_{xy}^p = \frac{\dot{\tau}_{xy}}{G} + \dot{\lambda}\frac{3\tau_x}{\sigma_0}, \end{aligned} \tag{3.2}$$

where $\dot{\lambda} > 0$, $F \leq 0$, $\dot{\lambda}F = 0$. Here 'dot' denotes the rate with respect to the process evolution parameter, such as increasing axial strain, E and G are the elastic Young and Kirchhoff moduli and σ_0 denotes the yield stress.

Neglecting elastic strains, from (3.2) we have

$$\dot{\varepsilon}_x = \dot{\varepsilon}_x^p = \dot{\lambda}\frac{\sigma_x}{\sigma_0}, \quad \dot{\gamma}_{xy} = \dot{\gamma}_{xy}^p = \dot{\lambda}\frac{3\tau_x}{\sigma_0}. \tag{3.3}$$

Inverting (3.3), the dissipation function can be specified, namely

$$\dot{D} = \sigma_x\dot{\varepsilon}_x^p + \tau_{xy}\dot{\gamma}_{xy}^p = \sigma_0\dot{\lambda} = \sigma_0\sqrt{(\dot{\varepsilon}_x^p)^2 + \frac{1}{3}(\dot{\gamma}_{xy}^p)^2}$$

and

$$\sigma_x = \frac{\partial\dot{D}}{\partial\dot{\varepsilon}_x^p} = \sigma_0\frac{\dot{\varepsilon}_x^p}{\sqrt{(\dot{\varepsilon}_x^p)^2 + \frac{1}{3}(\dot{\gamma}_{xy}^p)^2}}, \quad \tau_{xy} = \frac{\partial\dot{D}}{\partial\dot{\gamma}_{xy}^p} = \sigma_0\frac{\frac{1}{3}\dot{\gamma}_{xy}^p}{\sqrt{(\dot{\varepsilon}_x^p)^2 + \frac{1}{3}(\dot{\gamma}_{xy}^p)^2}} \tag{3.4}$$

For the piecewise-linear shear strain oscillation, Fig. 1c, we obtain from (3.4)

$$\sigma_x = \frac{\sigma_0}{\sqrt{1 + \frac{\eta^2}{3}}}, \quad \tau_{xy} = \pm\frac{\eta}{3}\frac{\sigma_0}{\sqrt{1 + \frac{\eta^2}{3}}} \tag{3.5}$$

and the specific dissipation power equals

$$\dot{D} = \sigma_0|\dot{\varepsilon}_x|\sqrt{1 + \frac{\eta^2}{3}} = \dot{D}_0\sqrt{1 + \frac{\eta^2}{3}}, \quad \dot{D}_0 = \sigma_0|\dot{\varepsilon}_x|. \tag{3.6}$$

For the harmonically varying shear strain, in view of (2.2), we obtain the stress components in the plastic state

$$\sigma_x = \frac{\sqrt{3}\sigma_0}{\sqrt{3+\eta^2\frac{\pi^2}{4}\cos^2(2\pi\frac{|\varepsilon_x|}{E_x})}}, \quad \tau_{xy} = \frac{\eta}{3}\frac{\sqrt{3}\sigma_0\eta^2\frac{\pi}{2}\cos(2\pi\frac{|\varepsilon_x|}{E_x})}{\sqrt{3+\eta^2\frac{\pi^2}{4}\cos^2(2\pi\frac{|\varepsilon_x|}{E_x})}} \tag{3.7}$$

and the dissipation power is expressed as follows

$$\dot{D} = \sigma_0|\dot{\varepsilon}_x|\sqrt{1+\eta^2\frac{\pi^2}{12}\cos^2(2\pi\frac{|\varepsilon_x|}{E_x})} = \dot{D}_0\sqrt{1+\eta^2\frac{\pi^2}{12}\cos^2(2\pi\frac{|\varepsilon_x|}{E_x})}. \tag{3.8}$$

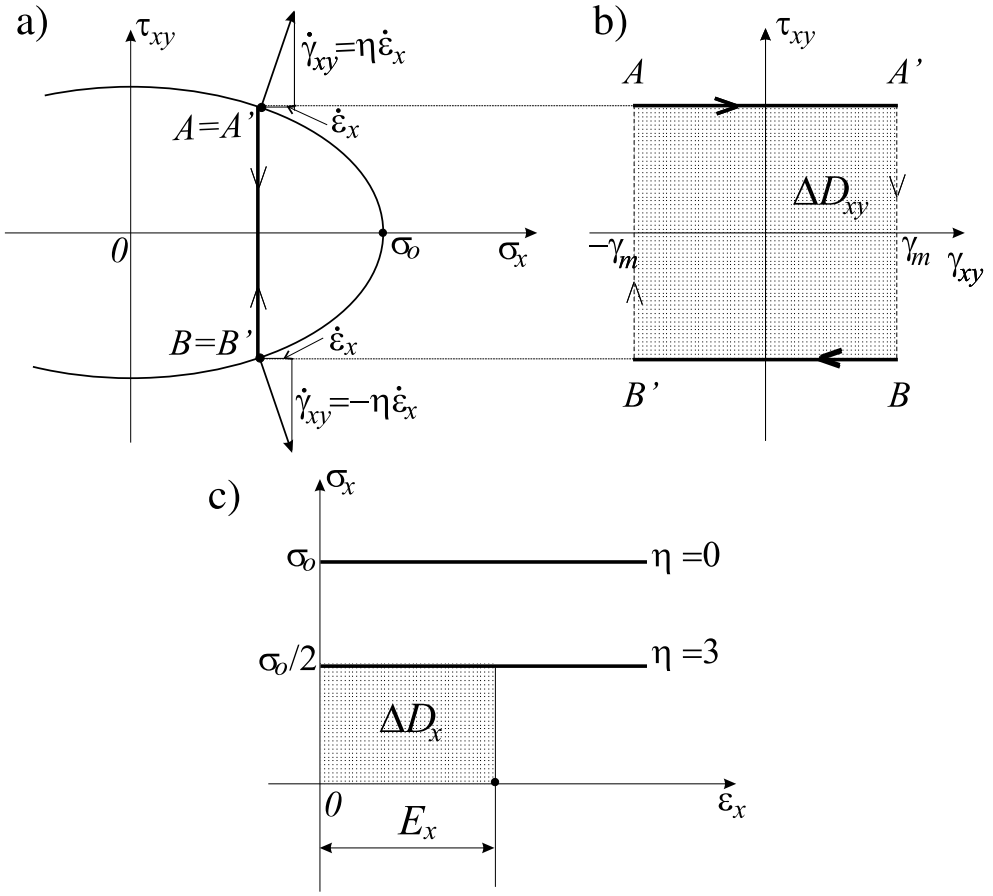

Figure 2. Piecewise linear shear strain control: a/ stress path, b/shear stress-strain hysteresis loop, c/axial stress variation

Some interesting conclusions can be drawn from this simple analysis. For the case of piecewise linear shear strain control, the stress path AB at constant axial stress value corresponds to consecutive combined plastic flow periods followed by rigid unloading to a reverse shear straining point on the yield surface, Fig. 2a. The shear hysteresis loop is shown in Fig. 2b and the axial stress variation in Fig. 2c. It follows from (3.5) and (3.6) that the axial stress value depends on η and is always reduced but the dissipation power is increased. For instance, for

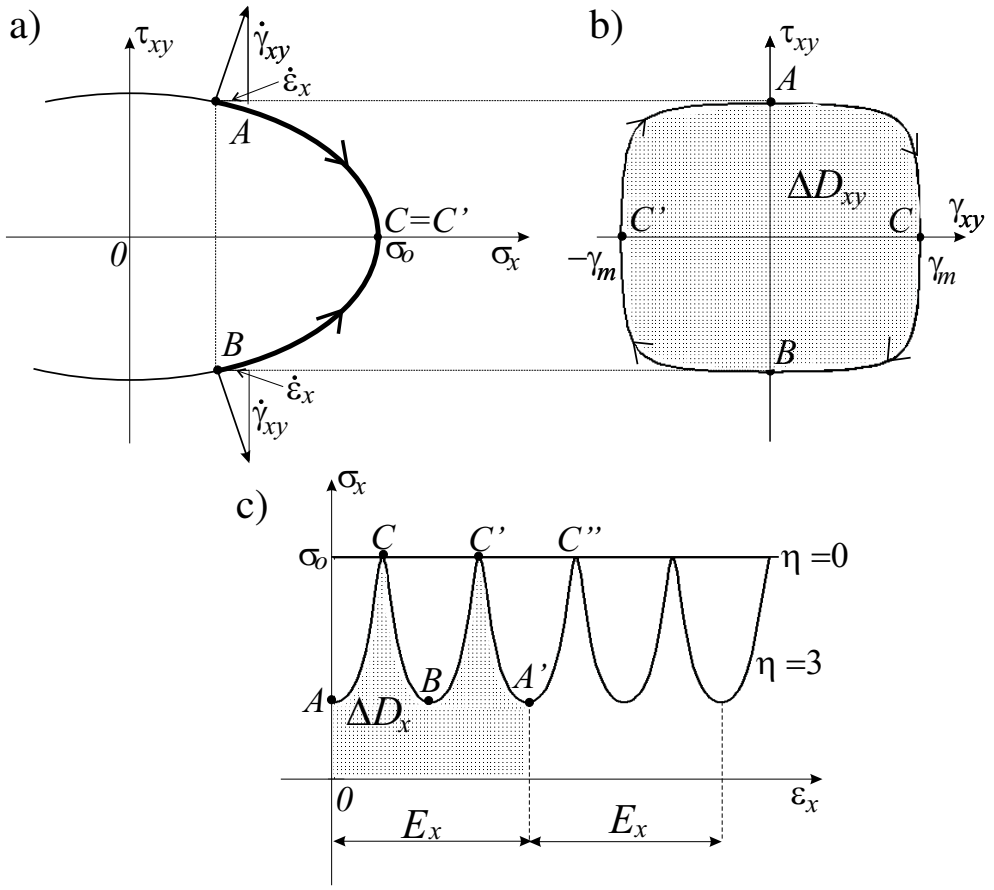

Figure 3. Harmonic shear strain control: a/ stress path, b/ shear stress-strain hysteresis loop, c/ axial stress variation

$\eta = 3$, there is $\sigma_x = \frac{1}{2}\sigma_0$ and $\dot{D} = 2\dot{D}_0 = 2\sigma_0|\dot{\varepsilon}_x|$. Thus, the axial stress reduction occurs at the expense of increasing dissipated energy in the deformation process.

The harmonic shear strain control provides a different stress path $ACBC'$ following the yield surface, Fig. 3a. Thus, there is no unloading stage and the deformation process proceeds in *a fully plastic regime*. The shear stress-strain hysteresis loop is shown in Fig. 3b. The axial stress varies between the values corresponding to A or B and the maximal value $\sigma = \sigma_0$ at C, Fig. 3c. The stress-strain path in Fig. 3c touches the line $\sigma = \sigma_0$ at C, C', C'', ... Note that this line corresponds to $\eta = 0$ that is to monotonic axial straining. The dissipation power increases with respect to its value $\dot{D}_0 = \sigma_0|\dot{\varepsilon}_x|$ corresponding to pure axial deformation.

To illustrate the dissipated energy variation with process parameters, let us calculate the dissipated energy in tension and torsion modes during one cycle of deformation. For the piecewise linear shear strain control in view of (3.5) we have

$$D_c^\gamma = \int_0^{cycle} \tau_{xy} d\gamma_{xy} = \frac{3}{4}\eta \frac{\sigma_0 \gamma_m}{\sqrt{1+\frac{1}{3}\eta^2}} = \sigma_0 E_x \frac{\frac{\eta^2}{3}}{\sqrt{1+\frac{\eta^2}{3}}}, \tag{3.9}$$

$$D_c^{\varepsilon} = \int_0^{cycle} \sigma_x d\varepsilon_x = \sigma_0 E_x \frac{1}{\sqrt{1+\frac{\eta^2}{3}}}, \tag{3.10}$$

where D_c^{γ} and D_c^{ε} are the dissipated energies in torsion and axial strain cycles. The total dissipated energy per cycle equals

$$D_c^t = D_c^{\gamma} + D_c^{\varepsilon} = \sigma_0 E_x \sqrt{1+\frac{\eta^2}{3}} = D_0^t \sqrt{1+\frac{\eta^2}{3}} \tag{3.11}$$

Similarly, introducing $e = |\varepsilon_x|/E_x$, for the case of harmonic control of shear strain, in view of (2.2), (3.7) and (3.8), we obtain

$$D_c^{\gamma} = \int_0^{cycle} \tau_{xy} d\gamma_{xy} = \sigma_0 E_x \int_0^1 \frac{\eta^2}{3} \frac{\frac{\pi^2}{4}\cos^2(2\pi e)}{\sqrt{1+\frac{\eta^2}{3}\frac{\pi^2}{4}\cos^2(2\pi e)}} de$$

$$D_c^{\varepsilon} = \int_0^{cycle} \sigma_x d\varepsilon_x = \sigma_0 E_x \int_0^1 \frac{1}{\sqrt{1+\frac{\eta^2}{3}\frac{\pi^2}{4}\cos^2(2\pi e)}} de$$

and

$$D_c^t = \sigma_0 E_x \int_0^1 \sqrt{1+\frac{\eta^2}{3}\frac{\pi^2}{4}\cos^2(2\pi e)}\, de$$

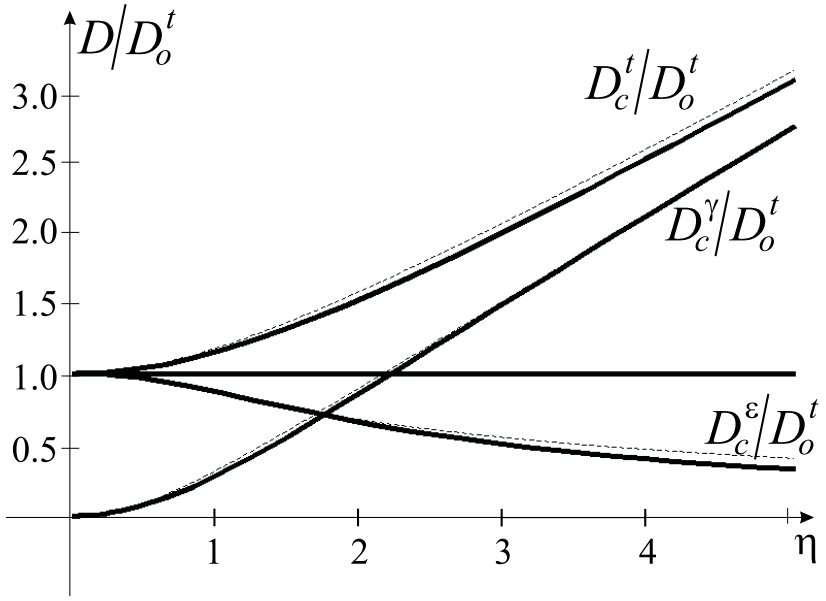

Figure 4. Variation of the dissipated energy in one deformation cycle with the strain rate ratio η: continuous line - piecewise linear shear strain control, dashed line - harmonic shear strain control

Figure 4 presents the variation of dissipated energies per one cycle in axial and torsional deformation. It is seen that the dissipated energy portion D_c^{ε} decreases with the increasing cycle frequency, but the dissipated energy D_c^{γ} increases. This leads to total dissipated energy increase with respect to the uniaxial deformation process.

4 Cyclic solution for an elastic-perfectly plastic material

Consider now the elastic-plastic material model for which the constitutive equations are specified by (3.1) and (3.2). We shall analyze both piecewise linear and harmonic shear strain controls.

4.1 Piecewise linear shear strain control: analytical solution

In view of the constraint $\dot{\gamma}_{xy}/\dot{\varepsilon}_x = \eta$, from (3.2) it follows that

$$\dot{\sigma}_x = E\left(\dot{\varepsilon}_x - \dot{\lambda}\frac{\sigma_x}{\sigma_0}\right), \quad \dot{\tau}_{xy} = G\left(\eta\dot{\varepsilon}_x - \dot{\lambda}\frac{3\tau_{xy}}{\sigma_0}\right). \tag{4.1}$$

For the plastic state, the consistency condition requires that

$$\dot{F} = \sigma_x\dot{\sigma}_x + 3\tau_{xy}\dot{\tau}_{xy} = 0. \tag{4.2}$$

Substituting (4.1) into (4.2), we obtain

$$\dot{\lambda} = \sigma_0\frac{E\sigma_x + 3G\eta\tau_{xy}}{E\sigma_x^2 + 9G\tau_{xy}^2}\dot{\varepsilon}_x, \quad \dot{\lambda} > 0, \quad \dot{\varepsilon}_x > 0. \tag{4.3}$$

Let us note that η takes positive and negative values, however, the shear stress τ_{xy} changes its sign with η, so we have $\tau_{xy} > 0$, $\eta > 0$ and $\tau_{xy} < 0$, $\eta < 0$, so that $\tau_{xy}\eta > 0$. The inverse elastic-plastic equations are

$$\begin{aligned}
\dot{\sigma}_x &= E\left(1 - \frac{E\sigma_x + 3G\eta\tau_{xy}}{E\sigma_x^2 + 9G\tau_{xy}^2}\sigma_x\right)\dot{\varepsilon}_x, \\
\dot{\tau}_{xy} &= G\left(\eta - \frac{E\sigma_x + 3G\eta\tau_{xy}}{E\sigma_x^2 + 9G\tau_{xy}^2}3\tau_{xy}\right)\dot{\varepsilon}_x
\end{aligned} \tag{4.4}$$

and for the elastic path we have

$$\dot{\sigma}_x = E\dot{\varepsilon}_x, \quad \dot{\tau}_{xy} = G\dot{\gamma}_{xy} = G\eta\dot{\varepsilon}_x.$$

To integrate analytically the rate equations (4.4), let us introduce the trigonometric stress representation satisfying the yield condition (3.1), namely

$$\sigma_x = \sigma_0\cos\theta, \quad \sqrt{3}\tau_{xy} = \sigma_0\sin\theta \tag{4.5}$$

with the rates

$$\dot{\sigma_x} = -\sigma_0(\sin\theta)\dot{\theta}, \quad \sqrt{3}\dot{\tau_{xy}} = \sigma_0(\cos\theta)\dot{\theta}. \tag{4.6}$$

The first incremental equation (4.4) can now be presented as follows

$$\frac{\sigma_0}{3G}\dot{\theta} = \frac{\frac{\sqrt{3}\eta}{3}\cos\theta - \sin\theta}{1 + \left(\frac{3G}{E} - 1\right)\sin^2\theta}\dot{\varepsilon}_x. \tag{4.7}$$

Let us introduce the following notation

$$\begin{aligned} \tan\Phi = \frac{\sqrt{3}|\eta|}{3} = \frac{\dot{\bar{\gamma}}_{xy}}{\dot{\bar{\varepsilon}}_x}, \quad m = \frac{3G}{E} - 1 = \frac{1-2\nu}{2(1+\nu)}, \\ \bar{\varepsilon}_x = \frac{E}{\sigma_0}\varepsilon_x = \frac{\varepsilon_x}{\varepsilon_0}, \quad \bar{\gamma}_{xy} = \frac{E}{\sigma_0}\frac{\gamma_{xy}}{\sqrt{3}}, \quad \tan\varphi = (1+m)\tan\Phi \end{aligned} \tag{4.8}$$

where $\varepsilon_0 = \sigma_0/E$ is the elastic strain in uniaxial tension associated with the yield stress σ_0. Equation (4.7) can now be rewritten in the incremental form

$$d\bar{\varepsilon}_x = \frac{\cos\Phi}{1+m}\frac{1 + m(\sin\theta)^2}{\sin(\pm\Phi - \theta)}d\theta. \tag{4.9}$$

Integrating (4.9), we obtain for $\eta > 0$

$$\bar{\varepsilon}_x = C + \underbrace{\frac{\cos\Phi}{1+m}\left[m\cos(\Phi+\theta) - (1 + m(\sin\Phi)^2)\ln\left|\tan\frac{\Phi-\theta}{2}\right|\right]}_{f(\theta)} \tag{4.10}$$

and for $\eta < 0$ we have

$$\bar{\varepsilon}_x = \bar{C} + \underbrace{\frac{\cos\Phi}{1+m}\left[m\cos(\Phi-\theta) - (1 + m(\sin\Phi)^2)\ln\left|\tan\frac{\Phi+\theta}{2}\right|\right]}_{f(-\theta)}, \tag{4.11}$$

where C and $\bar{C}$ are the integration constants obtained from the initial values on the respective paths.

The plastic strain rate $\dot{\varepsilon}_x^p$ is expressed as follows

$$\dot{\varepsilon}_x^p = \dot{\lambda}\cos\theta = \frac{\sigma_0^2}{E(1+m)}\frac{\cos\Phi}{\cos\varphi}\frac{\cos(\pm\varphi - \theta)}{\sin(\pm\Phi - \theta)}(\cos\theta)\dot{\theta} \tag{4.12}$$

Integrating (4.12), we obtain for $\eta > 0$

$$\bar{\varepsilon}_x^p = C_\varepsilon - \frac{\cos\Phi}{(1+m)\cos\varphi}\left[\cos(\varphi - \Phi - \theta) + \cos(\varphi - \Phi)\cos\Phi\ln|\tan(\frac{\Phi-\theta}{2})|\right]$$

and for $\eta < 0$ there is

$$\bar{\varepsilon}_x^p = \bar{C}_\varepsilon - \frac{\cos\Phi}{(1+m)\cos\varphi}\left[\cos(\varphi-\Phi+\theta) + \cos(\varphi-\Phi)\cos\Phi\ln|\tan(\frac{\Phi+\theta}{2})|\right],$$

where C_ε and $\bar{C}_\varepsilon$ denote the integration constants.

For the elastic path, we can write for $\eta > 0$

$$s_x = \frac{\sigma_x}{\sigma_0} = \frac{E\varepsilon_x}{\sigma_0} + s_0 = \bar{\varepsilon}_x + s_0, \tag{4.13}$$
$$s_{xy} = \frac{\sqrt{3}\tau_{xy}}{\sigma_0} = \frac{\sqrt{3}G\eta}{\sigma_0}\varepsilon_x + t_0 = \tan\varphi\bar{\varepsilon}_x + t_0$$

and for $\eta < 0$, there is

$$s_x = \frac{\sigma_x}{\sigma_0} = \frac{E\varepsilon_x}{\sigma_0} + s_0 = \bar{\varepsilon}_x + s_0, \tag{4.14}$$
$$s_{xy} = \frac{\sqrt{3}\tau_{xy}}{\sigma_0} = -\frac{\sqrt{3}G\eta}{\sigma_0}\varepsilon_x + t_0 = -\tan\varphi\bar{\varepsilon}_x + t_0$$

Now, let us specify the rate of plastic dissipation. During one cycle of deformation the elastic work vanishes and the work of external loading is dissipated. We have

$$\dot{D} = \sigma_x\dot{\varepsilon}_x^p + \tau_{xy}\dot{\gamma}_{xy}^p = \sigma_0\dot{\lambda} = \dot{D}_x + \dot{D}_{xy}. \tag{4.15}$$

In view of (4.5) and (4.3) we obtain

$$\dot{D} = \frac{\sigma_0^2}{E(1+m)}\frac{\cos\Phi}{\cos\varphi}\frac{\cos(\varphi\mp\theta)}{\sin(\pm\Phi-\theta)}\dot{\theta}$$

and

$$\dot{D}_x = \sigma_0\dot{\lambda}\cos^2\theta = \dot{W}^p\cos^2\theta, \quad \dot{D}_{xy}^p = \sigma_0\dot{\lambda}\sin^2\theta = \dot{W}^p\sin^2\theta.$$

Denoting

$$\bar{D} = \frac{D}{D_0}, \quad D_0 = \sigma_0\varepsilon_0$$

and integrating (4.15), we obtain for $\eta > 0$

$$\bar{D}(\theta) = C_w - \frac{\cos\Phi}{(1+m)\cos\varphi}\left[\cos(\varphi-\Phi)\ln|\sin(\Phi-\theta)| + \theta\sin(\varphi-\Phi)\right] \tag{4.16}$$

and for $\eta < 0$ there is

$$\bar{D}(\theta) = \bar{C}_w - \frac{\cos\Phi}{(1+m)\cos\varphi}\left[\cos(\varphi-\Phi)\ln|\sin(\Phi+\theta)| - \theta\sin(\varphi-\Phi)\right] \tag{4.17}$$

where C_w and $\bar{C}_w$ denote the integration constants calculated from the accumulated value in the previous cycles. The tensile and torsional dissipated energies are

$$\bar{D}_x(\theta) = C_{wx} - \frac{1}{4}\frac{\cos\Phi}{(1+m)\cos\varphi}\left[\cos(\pm\varphi \mp \Phi - 2\theta)\right. \\ \left. + A(\pm\Phi, \pm\varphi)\ln|\sin(\pm\Phi - \theta)| + \theta B(\pm\Phi, \pm\varphi)\right], \tag{4.18}$$

where

$$A(\Phi, \varphi) = \cos(\varphi + \Phi) + \cos(\varphi - 3\Phi) + 2\cos(\varphi - \Phi),$$

$$B(\Phi, \varphi) = \sin(\varphi - 3\Phi) + 2\sin(\varphi - \Phi) - \sin(\varphi + \Phi)$$

and

$$\bar{D}_{xy}(\theta) = C_{wxy} + \frac{1}{4}\frac{\cos\Phi}{(1+m)\cos\varphi}\left[\cos(\pm\varphi \mp \Phi - 2\theta)\right. \\ \left. + C(\pm\Phi, \pm\varphi)\ln|\sin(\pm\Phi - \theta)| + \theta D(\pm\Phi, \pm\varphi)\right], \tag{4.19}$$

where

$$C(\Phi, \varphi) = \cos(\varphi + \Phi) + \cos(\varphi - 3\Phi) - 2\cos(\varphi - \Phi),$$

$$D(\Phi, \varphi) = \sin(\varphi - 3\Phi) - 2\sin(\varphi - \Phi) - \sin(\varphi + \Phi).$$

4.2 Analysis of process parameters

Consider now the steady state cyclic deformation process for specified γ_m and η. Figure 5a presents one of typical steady cyclic states in the stress plane $s_x = \sigma_x/\sigma_0$, $s_{xy} = \sqrt{3}\tau_{xy}/\sigma_0$. The yield condition is now represented by a circle of unit radius and the conjugate plastic strain rates are $\dot{\varepsilon}^p_x$ and $\dot{\gamma}^p_{xy}/\sqrt{3}$.

The cyclic stress path is formed by two semi-cycles $O^* - D - A - O^*$ and $O^* - B - C - O^*$, where the position O^* is specified by the value $s_x = s^*$ which is to be determined. The elastic stress paths AB and CD are inclined at the angle φ to the s_x-axis, where for positive η

$$\tan\varphi = \frac{\dot{s}_{xy}}{\dot{s}_x} = \frac{\sqrt{3}\dot{\tau}_{xy}}{\dot{\sigma}_x} = (1+m)\tan\Phi = \left(\frac{3}{2}\frac{1}{1+\nu}\right)\frac{\eta}{\sqrt{3}}$$

and the angle Φ specifies the elastic or purely plastic strain path for transformed strains $\bar{\varepsilon}_x$ and $\bar{\gamma}_{xy}$. Note that $\varphi > \Phi$ for $\nu \le 0.5$. The radial lines $O - A$ and $O - D$ are inclined at the angles θ_A and θ_D to the s_x - axis. From geometrical relations it is seen that

$$\Delta\theta = \theta_A - \theta_D = \pi - 2\varphi, \tag{4.20}$$

$$\tan\theta_A = \frac{\sin\varphi\sqrt{1 - (s^*)^2\sin^2\varphi} - s^*\cos\varphi}{\cos\varphi\sqrt{1 - (s^*)^2\sin^2\varphi} + s^*\sin^2\varphi}. \tag{4.21}$$

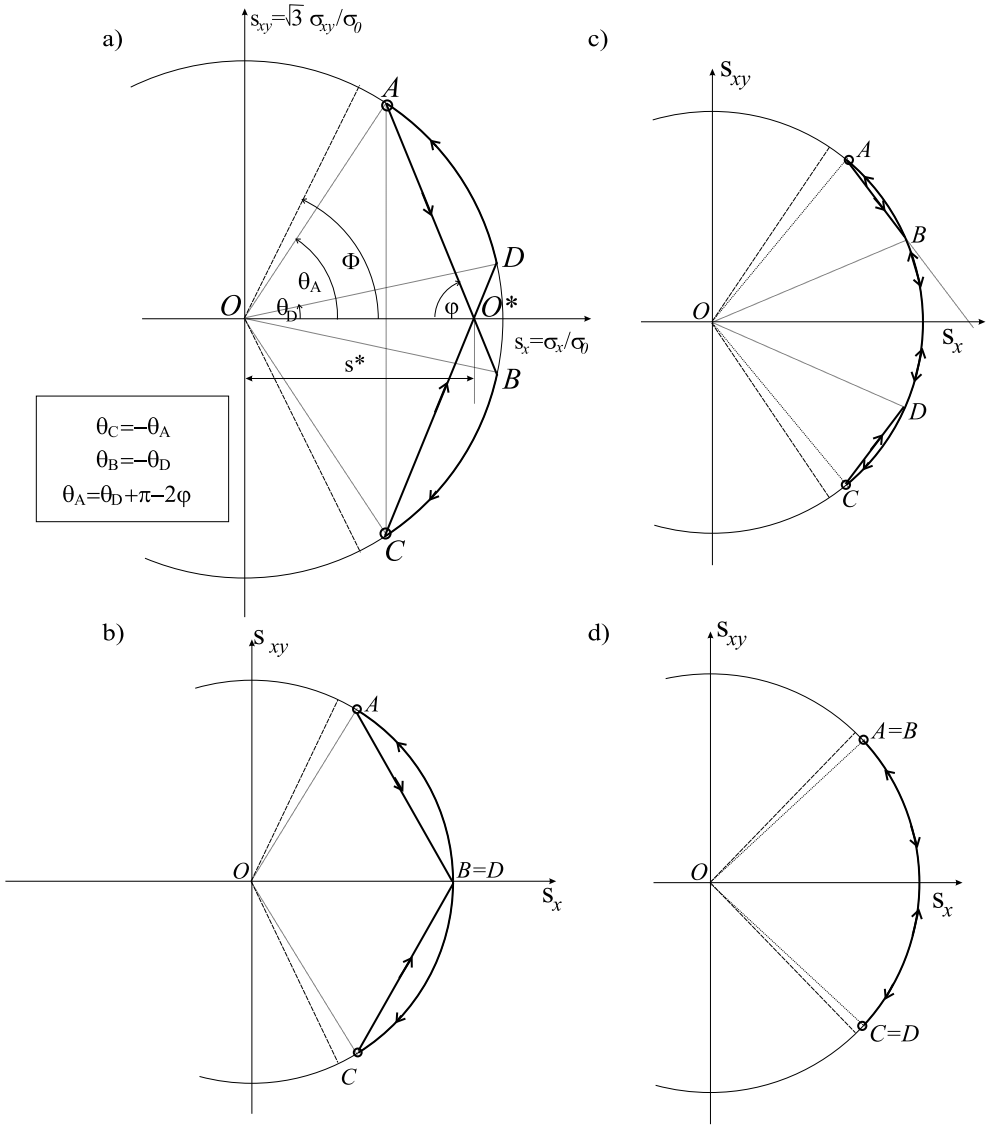

Figure 5. Steady state cycles representation in the s_x, s_{xy}-plane a/ the case $\eta > \eta_m(\gamma_m)$, b/ the case $\eta = \eta_m(\gamma_m)$, c/ the case $\eta_l(\gamma_m) < \eta < \eta_m(\gamma_m)$, d/ the case $\eta > \eta_l(\gamma_m)$

Let us specify first the limit value of η for which the elastic unloading or reloading occurs along the path AB or CD. The unloading inequality is

$$\dot{F} = \sigma_x \dot{\sigma}_x + 3\tau_{xy}\dot{\tau}_{xy} = \sigma_x(E\dot{\varepsilon}_x) + 3\tau_{xy}(-G|\eta|\dot{\varepsilon}_x) \leq 0,$$

where $\sigma_x = \sigma_0 \cos\theta_A$, $3\tau_{xy} = \sqrt{3}\sigma_0 \sin\theta_A$. We have

$$\dot{F} = \left(\cos\theta_A - \sqrt{3}\sin\theta_A \frac{G}{E}\eta\right)\sigma_0 E\dot{\varepsilon}_x = \left(1 - (2+m)(\sin\Phi)^2\right)\sigma_0 E\dot{\varepsilon}_x \leq 0 \quad (4.22)$$

where we assumed the limit value of $\theta_A = \Phi$ occurring for $\gamma_m \to \infty$. For finite

shear amplitude values, there should be $\theta_A < \Phi$. The inequality (4.22) provides

$$|\eta| \geq \sqrt{\frac{3}{1+m}} = \eta_{l(\infty)}$$

and for finite values of γ_m the corresponding limit value $\eta_l = \eta_l(\gamma_m)$ should be greater than $\eta_{l(\infty)}$ thus

$$\eta_l(\gamma_m) > \eta_{l(\infty)}.$$

The other steady cycle pattern can be generated when the points D and B merge on the s_x-axis, Fig. 5b. Then, the maximal axial stress reached in the cyclic process equals the static value σ_0. Considering the elastic path from A and assuming it touches the yield surface at B, we can write

$$\begin{aligned} s_x &= \bar{\varepsilon}_x^* + \cos\theta_A = 1 \\ s_{xy} &= -\tan\varphi\bar{\varepsilon}_x^* + \sin\theta_A = 0. \end{aligned}$$

We note also that $\theta_A = \pi - 2\varphi$ along the path AB. In the case $\gamma_m \to \infty$ the angle θ_A can be replaced by Φ and we obtain the condition for the maximal stress σ_x to be less or equal to σ_0

$$|\eta| \geq \frac{\sqrt{3(3+2m)}}{1+m} = \eta_{m(\infty)}$$

Here again for a finite value of γ_m, the corresponding value $\eta_m = \eta_m(\gamma_m)$ is greater than $\eta_{m(\infty)}$ thus $\eta_m(\gamma_m) > \eta_{m(\infty)}$. After reaching the yield stress at B the stress path remains on the yield surface and at the instant of reversing the twist the stress state is represented by point C which is a mirror image of point A with respect to the s_x-axis. When the elastic unloading occurs, the yield surface is reached again at the point D which is the mirror reflection of point B, Fig. 5a. The maximal value of the tensile stress s_{max} reached in the course of deformation process is represented by points B and D. When $\eta = \eta_m$, then $s_{max} = 1$ and points B and D merge on the s_x-axis.

Figure 6 presents the variation of angle difference $\varphi - \Phi$ for increasing values of η and different values of the Poisson ratio. It is seen that $\varphi - \Phi$ reaches a maximum for η close to 2 and then tends to 0. The characteristic material parameters and two limit values of η for different metallic materials are collected in Table 1 [1]. It is seen that η_l and η_m vary within very small range.

Fig. 5c presents the case when the yield point at D is reached by the elastic unloading path AB for $s_{xy}(B) > 0$ and similarly the point D is reached for $s_{xy}(D) < 0$. This case corresponds to $\eta_l(\gamma_m) \leq \eta \leq \eta_m(\gamma_m)$. Fig. 5d presents the

[1] Material parameters in Table 1 are collected on the basis of *A concise encyclopedia of metallurgy* ed. A.D. Merriman and *Vademecum of Material Science* [In Polish], W. Domke, WNT, Warszawa, 1982

Metal	E [GPa]	σ_0 [MPa]	ε_0 [%]	ν	m	η_m	η_l
Al	68.3	13-22	0.02-0.03	0.34	0.119	2.785	1.637
Al-alloy	70	40-320	0.06-0.45	0.33	0.128	2.771	1.631
Sn	54.3	34.5*	0.06*	0.36	0.103	2.812	1.649
Zn	86.9	110*	0.13*	0.25	0.200	2.661	1.581
Cu(annealed)	123	40-80	0.03-0.06	0.35	0.111	2.798	1.643
Pb	16.2	12.5*	0.08*	0.44	0.042	2.920	1.697
Ag	79.5	276*	0.35*	0.37	0.095	2.825	1.655
Ti	110	170	0.15	0.36	0.103	2.812	1.649
Au	80	138*	0.17*	0.44	0.042	2.920	1.697
cast iron	211	80-150	0.04-0.07	0.27	0.181	2.689	1.594
mild steel	210	130-350	0.06-0.17	0.29	0.163	2.716	1.606
stainless steel	210	500-680	0.24-0.33	0.3	0.154	2.730	1.612

Table 1
Values of material parameters and two limit values of η for different metallic materials (values denoted with a star specify the tensile strength). For Al-alloys, cast iron and steels the yield stress strongly depends on the steel composition and the forming process

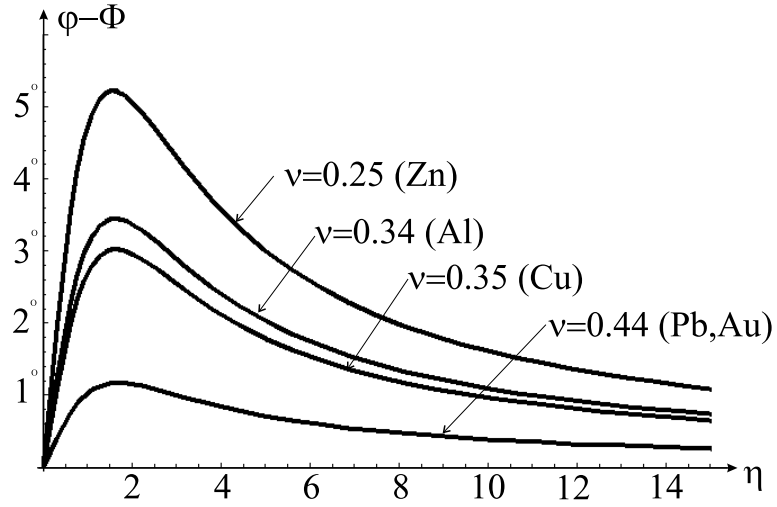

Figure 6. Difference $\varphi - \Phi$ for varying η and different values of ν

stress path for which there is no elastic unloading and the whole deformation process is purely plastic. This occurs when $\eta \leq \eta_l(\gamma_m)$.

Let us now provide the solution for the half-cycle of the steady state of cyclic deformation presented in Fig. 5a. At the point A we have $\bar{\varepsilon}_x(A) = \bar{\varepsilon}_A$, $\bar{\gamma}_{xy}(A) = \bar{\gamma}_m$, $\bar{\varepsilon}_x = \bar{\varepsilon}_A + \Delta\bar{\varepsilon}_x$. Along the path portion AB the elastic deformation occurs

and we have

$$s_x = \Delta\bar{\varepsilon}_x + \cos\theta_A \tag{4.23}$$
$$s_{xy} = -\tan\varphi\Delta\bar{\varepsilon}_x + \sin\theta_A. \tag{4.24}$$

Along the stress path portion BC the elastic-plastic deformation occurs, and we have in view of (4.10)

$$\begin{aligned}\bar{E}_x/2 = \Delta\bar{\varepsilon}_x(\theta_C) &= \cos\theta_B - \cos\theta_A - f(-\theta_B) + f(-\theta_C) = \\ &= \cos\theta_D - \cos\theta_A - f(\theta_D) + f(\theta_A)\end{aligned}$$

and finally

$$\bar{\gamma}_m = \frac{\eta}{2}\left(\cos\theta_D - \cos\theta_A - f(\theta_D) + f(\theta_A)\right). \tag{4.25}$$

On the other hand, when no elastic unloading occurs, this relation simplifies to

$$\bar{\gamma}_m = \frac{\eta}{2}\left(f(\theta_A) - f(-\theta_A)\right) \tag{4.26}$$

Equations (4.25) and (4.26) provide the solution for steady cyclic states. In fact, as $\theta_D = \theta_A - (\pi - 2\varphi)$, $\cos\theta_D = -\cos(\theta_A + 2\varphi)$, Eq. (4.25) can be rewritten in the form

$$\bar{\gamma}_m = \frac{\eta}{2}\left(-\cos(\theta_A + 2\varphi) - \cos\theta_A - f(\theta_A + 2\varphi - \pi) + f(\theta_A)\right). \tag{4.27}$$

This equation can be solved numerically for specified $\bar{\gamma}_m$ and η thus providing θ_A, θ_D and $\theta_B = -\theta_D$, $\theta_C = -\theta_A$. For purely plastic regime Eq. (4.26) provides the solution for θ_A.

Now, let us specify the limit response curves $\eta_l = \eta_l(\gamma_m)$ and $\eta_m = \eta_m(\gamma_m)$ separating in the plane of process parameters η, γ_m the domains of different responses with stress paths shown in Fig. 5. The curve $\eta_m = \eta_m(\gamma_m)$ separates the domains $\mathcal{C}$ and $\mathcal{B}$. In the domain $\mathcal{C}$ both elastic unloading or reloading tensile paths AB and CD occur with reduction of maximal stress with respect to the limit value $\sigma_x = \sigma_0$ cf. Fig. 5a. In the domain $\mathcal{B}$, the elastic unloading and reloading paths AB and CD exist, but the maximal value of tensile stress equals σ_0, cf. Fig. 5. The curve $\eta_l = \eta_l(\gamma_m)$ separates the domains $\mathcal{B}$ and $\mathcal{A}$, where in the domain $\mathcal{A}$ no elastic unloading or reloading occurs, cf. Fig. 5d. As for the case of purely plastic cycle there is $\theta_D = -\theta_A$, we have, in view of the relation $\theta_D = \theta_A - (\pi - 2\varphi)$, the value of $\theta_A = \pi/2 - \varphi = -\theta_D$ and the limit line $\eta_l = \eta_l(\gamma_m)$ is specified by the relation

$$\bar{\gamma}_m = \frac{\eta_l}{2}\left(f(\frac{\pi}{2} - \varphi) - f(\varphi - \frac{\pi}{2})\right).$$

The response curve $\eta_m = \eta_m(\gamma_m)$ separating the domains $\mathcal{C}$ and $\mathcal{B}$ is specified

setting $\theta_D = 0$ and $\theta_A = \pi - 2\varphi$ into Eq. (4.25) which provides

$$\bar{\gamma}_m = \frac{\eta_m}{2}\left(1 + \cos(2\varphi) - f(0) + f(\pi - 2\varphi)\right).$$

Figure 7 provides the three response domains in the plane $(\eta, \gamma_m/\varepsilon_0)$. Let us note that the separating curves tend to asymptotic values $\eta_{l(\infty)}$ and $\eta_{m(\infty)}$ for $\gamma_m \to \infty$.

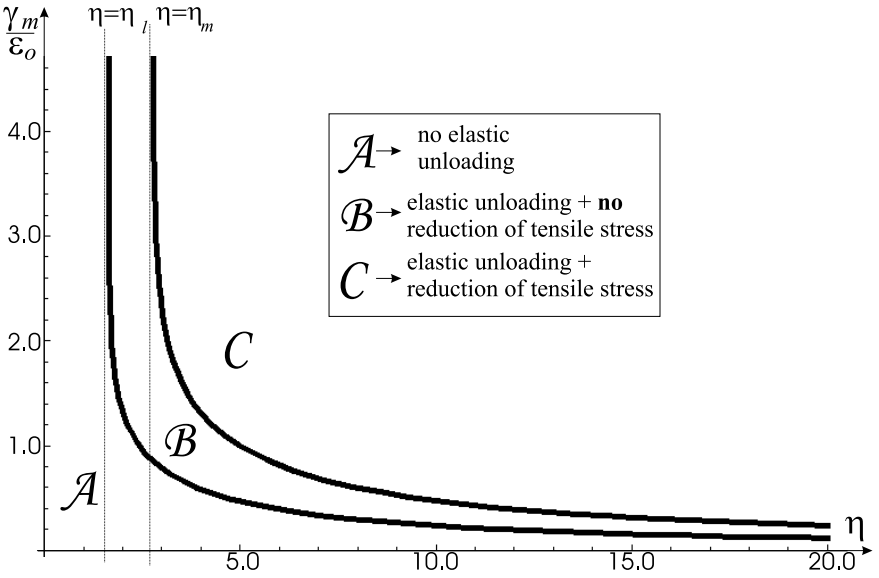

Figure 7. The regimes $\mathcal{A}$, $\mathcal{B}$, $\mathcal{C}$ of cyclic response in the plane of process parameters η, γ_m ($m = m_{Al} = 0.128$).

Let us note that for the regime $\mathcal{C}$ where the elastic unloading or reloading occurs, we have

$$s_{max} = \cos\theta_D = -\cos(\theta_A + 2\varphi), \quad s^* = \frac{\sin(\theta_A + \varphi)}{\sin\varphi}, \quad s_{min} = \cos\theta_A$$

and for the remaining two regimes $\mathcal{A}$ and $\mathcal{B}$ there is

$$s_{max} = s^* = 1, \quad s_{min} = \cos\theta_A$$

so the angle θ_A could be easily related to s_{min}.

Figure 8 presents the distribution of isolines $s_{min} = const$ in the response plane $(\eta, \gamma_m/\varepsilon_0)$. The curves separating domains $\mathcal{A}$, $\mathcal{B}$, $\mathcal{C}$ are also shown in bold lines. It is seen that the curves are bounded by the asymptotic lines for $\gamma_m \to \infty$ and $\eta \to \infty$ thus

$$\eta_l^{s_{min}} = \frac{\sqrt{3(1 - s_{min}^2)}}{s_{min}}, \quad \bar{\gamma}_m^{s_{min}} = \frac{\sqrt{3(1 - s_{min}^2)}}{1 + m}$$

Figure 9 presents the distribution of isolines $s_{max} = const$ The domains $\mathcal{A}$ and $\mathcal{B}$ for which $s_{max} = 1$ is marked below the separating curve $\eta_m = \eta_{m(\infty)}$. It is

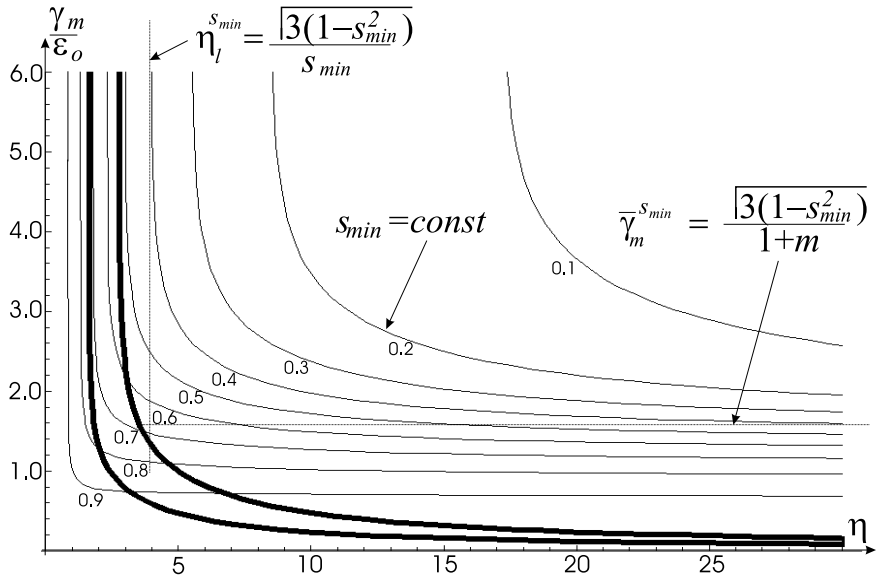

Figure 8. Minimal values s_{min} of the tensile stress in the plane of process parameters η, γ_m. Bold lines separate the regimes $\mathcal{A}$, $\mathcal{B}$, $\mathcal{C}$ ($m = m_{Al} = 0.128$).

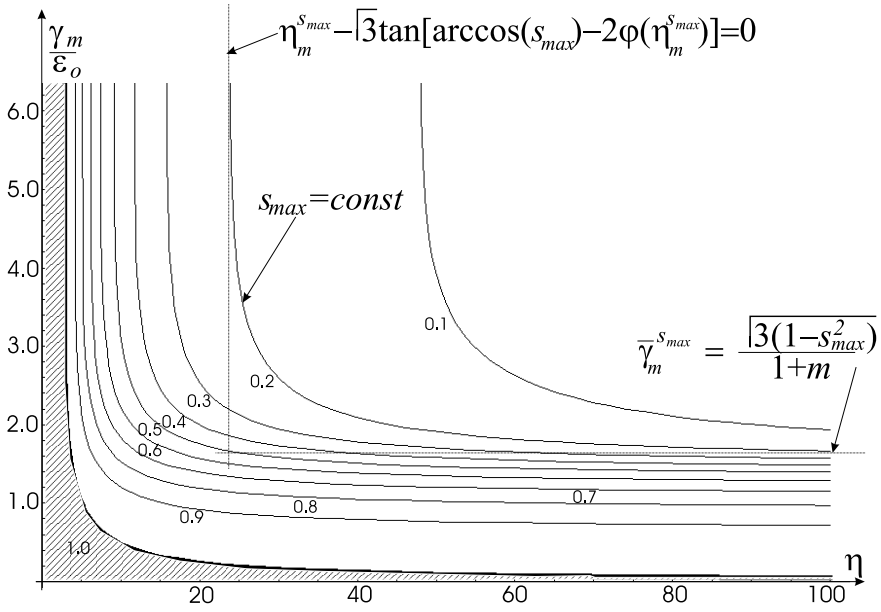

Figure 9. Maximal values s_{max} of the tensile stress in the space of process parameters η, γ_m. Bold line separates the regime $\mathcal{C}$ and regimes $\mathcal{A}$, $\mathcal{B}$ of no maximal stress reduction, ($m = m_{Al} = 0.128$).

seen that the isolines $s_{max} = const$ tend to asymptotic values for $\gamma_m \to \infty$ and $\eta \to \infty$, satisfying the relations

$$\bar{\gamma}_m^{s_{max}} = \frac{\sqrt{3(1-s_{max}^2)}}{1+m}, \quad \eta_l^{s_{max}} - \sqrt{3}\tan\left[\arccos(s_{max}) - 2\varphi(\eta_m^{s_{max}})\right] = 0$$

The typical axial and torsional cyclic responses for different values of η and $\bar{\gamma}_m$

are illustrated in Figs. 10-12.

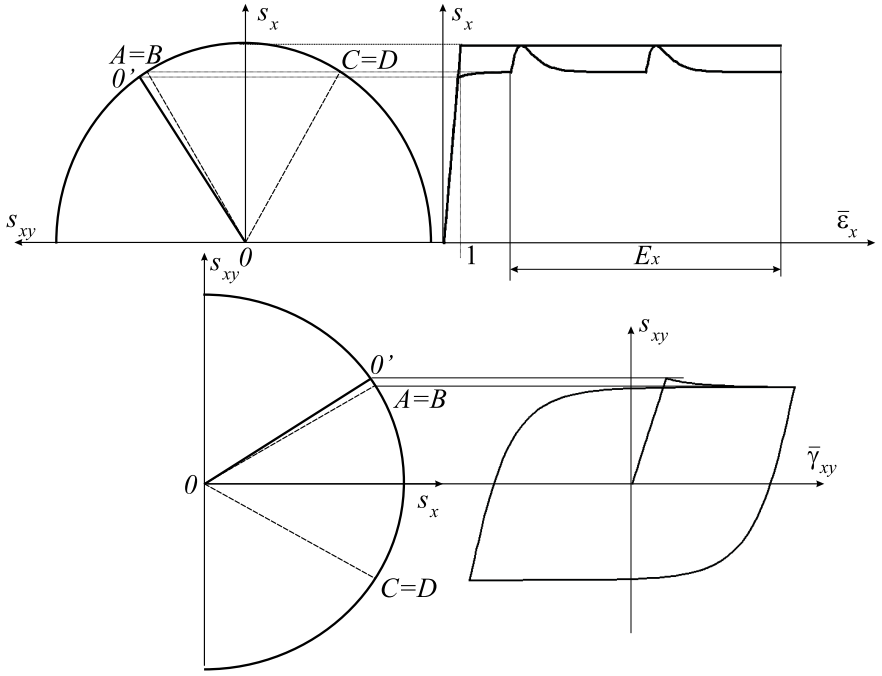

Figure 10. Variation of the tensile stress path and the hysteresis loop of shear stress-strain response in the course of cyclic deformation, $\eta < \eta_l$ regime $\mathcal{A}$: no elastic unloading

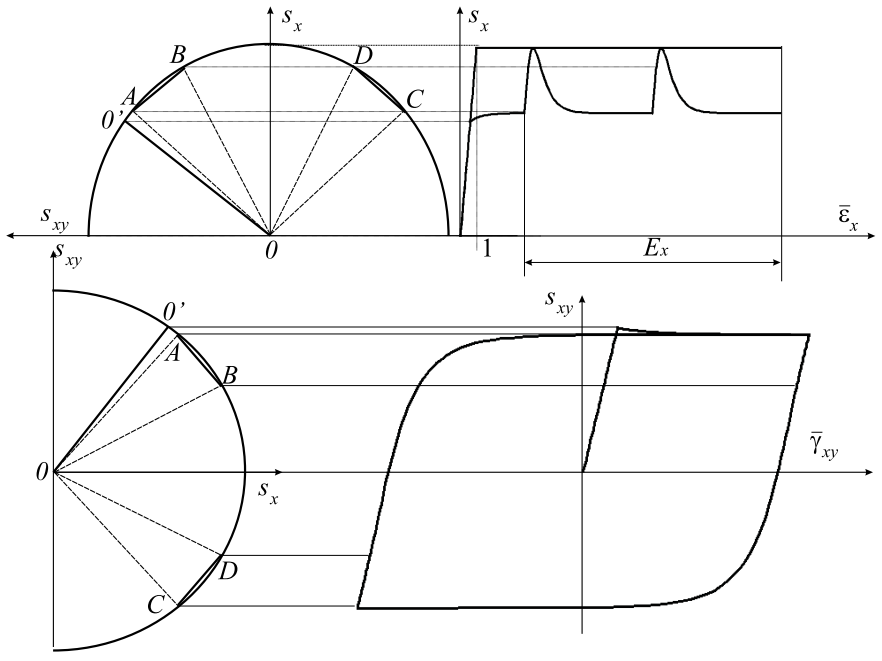

Figure 11. Variation of the tensile stress path and the hysteresis loop of shear stress-strain response in the steady cyclic deformation, $\eta_l < \eta < \eta_m$ regime $\mathcal{B}$: elastic unloading no reduction of s_{max}

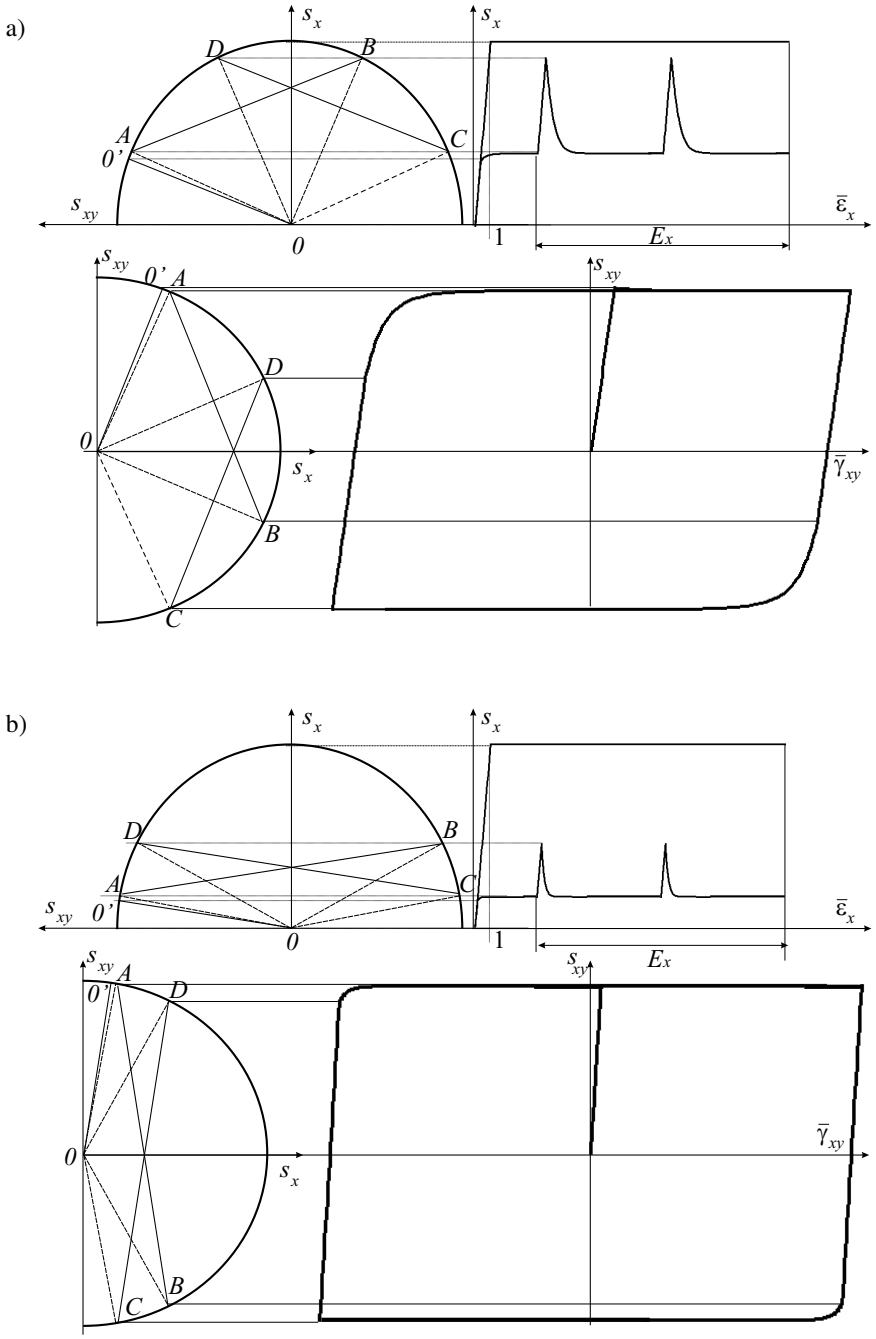

Figure 12. Variation of the tensile stress path and the hysteresis loop of shear stress-strain response in the steady cyclic deformation, $\eta > \eta_m$: a/ $\eta = 4$, b) $\eta = 10$ (regime $\mathcal{C}$: elastic unloading, maximal tensile stress reduction)

Consider now the plastic dissipation generated in one deformation cycle. Following (4.16), (4.17) and (4.18), (4.19), we may calculate the total dissipation $\Delta\bar{D}$, and the portions $\Delta\bar{D}_x$, $\Delta\bar{D}_{xy}$. Fig. 13 presents the variation of dissipation increments for increasing values of η. It is seen that the total dissipation increment largely increases with respect to the dissipation increment in pure tension. However, the tensile dissipation increment decreases and tends to zero for

increasing values of η.

The increment of plastic dissipation during one cycle when $\theta_A \to \Phi$ (for sufficiently large values of E_x and γ_m) may be calculated as a double increment of plastic dissipation during the half-cycle, so that

$$\Delta\bar{D}_{cycle} = 2(\bar{D}(\theta_A) - \bar{D}(\theta_D)) = 2(\bar{D}(\theta_A) - \bar{D}(\theta_A - \pi + 2\varphi))$$

for an elastic-plastic half-cycle and

$$\Delta\bar{D}_{cycle} = 2(\bar{D}(\theta_A) - \bar{D}(-\theta_A)).$$

for a totally plastic semicycle. Let us note that the angle θ_A is uniquely related with γ_m, η and E_x for the steady cycle, Eqs. (4.26), (4.27).

Similarly we may calculate the increment of the axial plastic strain $\bar{\varepsilon}_x^P$ during one steady cycle respectively for two regimes, so we have

$$\Delta\bar{\varepsilon}^P_{cycle} = 2(\bar{\varepsilon}^p_x(\theta_A) - \bar{\varepsilon}^p_x(\theta_A - \pi + 2\varphi)),$$

$$\Delta\bar{\varepsilon}^P_{cycle} = 2(\bar{\varepsilon}^p_x(\theta_A) - \bar{\varepsilon}^p_x(-\theta_A)).$$

Let the ratio $\delta = \frac{\Delta\bar{D}_{cycle}}{\Delta\bar{\varepsilon}^P_{cycle}}$ of a plastic work increment and a plastic strain increment during one cycle be treated as a energy-based measure of expense of the plastic extension process. For the pure tension this *expense coefficient* δ equals to one.

It would be interesting to find the upper limit value of δ for arbitrary values of η but for $\gamma_m \to \infty$ what is equivalent to $\theta_A \to \Phi$. We obtain (as compared to the results (3.9)-(3.11))

$$\delta_l = \lim_{\theta_A\to\Phi} \frac{\Delta\bar{D}_{cycle}}{\Delta\bar{\varepsilon}^P_{cycle}} = \lim_{\theta_A\to\Phi} \frac{\bar{D}(\theta_A) - \bar{D}(\theta_A - \pi + 2\varphi)}{\bar{\varepsilon}^p_x(\theta_A) - \bar{\varepsilon}^p_x(\theta_A - \pi + 2\varphi)} = \tag{4.28}$$

$$= \lim_{\theta_A\to\Phi} \frac{\frac{d\bar{D}}{d\theta}}{\frac{d\bar{\varepsilon}^p}{d\theta}} = \frac{1}{\cos\Phi} = \sqrt{1 + \frac{\eta^2}{3}}$$

and similarly

$$\lim_{\theta_A\to\Phi} \frac{\Delta\bar{Dx}_{cycle}}{\Delta\bar{\varepsilon}^P_{cycle}} = \cos\Phi = \frac{1}{\sqrt{1 + \frac{\eta^2}{3}}}, \tag{4.29}$$

$$\lim_{\theta_A\to\Phi} \frac{\Delta\bar{Dxy}_{cycle}}{\Delta\bar{\varepsilon}^P_{cycle}} = \frac{1}{\cos\Phi} - \cos\Phi = \frac{\frac{1}{3}\eta^2}{\sqrt{1 + \frac{\eta^2}{3}}}. \tag{4.30}$$

Fig. 13a presents the variation of the expense coefficient for varying values of η and E_x. Figs 13b,c present the evolution of axial and torsional expense coefficients. The bold lines present the limit values derived analytically, cf. Eqs (4.28-4.30). It is seen that the total dissipation always increases for the combined process, however, the axial dissipation decreases remarkably for increasing values of η and γ_m.

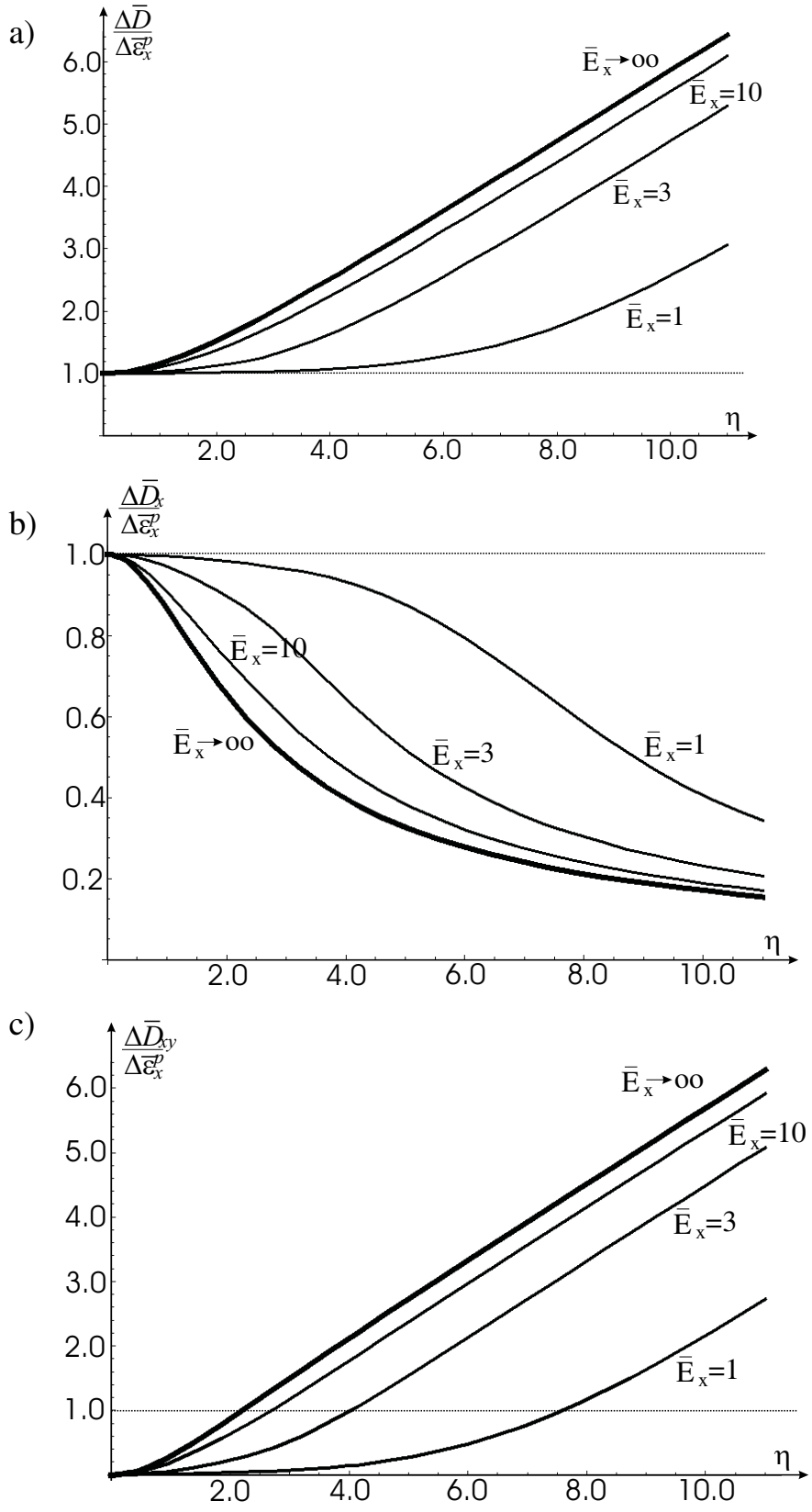

Figure 13. a/ Variation of the ratio of total plastic dissipation increment per cycle and the axial plastic strain increment (expense coefficient δ) with E_x and η , b/ variation of axial expense coefficient c/ variation of torsional expense coefficient.

4.3 Harmonic shear strain control: incremental relations

Consider now the harmonic shear strain control specified by (2.2), accompanied by the progressive axial extension, thus

$$\dot{\varepsilon}_x = \dot{\alpha}, \quad \frac{\dot{\gamma}_{xy}}{\dot{\varepsilon}_x} = \eta\frac{\pi}{2}\cos\left(2\pi\frac{\varepsilon_x}{E_x}\right). \tag{4.31}$$

For the elastic regime, the incremental (or rate) equations are

$$\dot{\sigma}_x = E\dot{\varepsilon}_x, \quad \dot{\tau}_x = G\eta\frac{\pi}{2}\cos\left(2\pi\frac{\varepsilon_x}{E_x}\right)\dot{\varepsilon}_x. \tag{4.32}$$

and for the elastic-plastic regime we have

$$\dot{\sigma}_x = E\left(\dot{\varepsilon}_x - \dot{\lambda}\frac{\sigma_x}{\sigma_0}\right), \quad \dot{\tau}_{xy} = G\left(\eta\frac{\pi}{2}\cos\left(2\pi\frac{\varepsilon_x}{E_x}\right)\dot{\varepsilon}_x - \dot{\lambda}\frac{3\tau_{xy}}{\sigma_0}\right) \tag{4.33}$$

The yield condition (3.1) and the consistency condition $\dot{F} = 0$ provide

$$\dot{\lambda} = \sigma_0\frac{E\sigma_x + 3G\eta\frac{\pi}{2}\cos\left(2\pi\frac{\varepsilon_x}{E_x}\right)\tau_{xy}}{E\sigma_x^2 + 9G\tau_{xy}^2}\dot{\varepsilon}_x \tag{4.34}$$

and the relations (4.33) can be written in the form

$$\begin{aligned}
\dot{\sigma}_x &= E\left(1 - \frac{E\sigma_x + 3G\eta\frac{\pi}{2}\cos\left(2\pi\frac{\varepsilon_x}{E_x}\right)\tau_{xy}}{E\sigma_x^2 + 9G\tau_{xy}^2}\sigma_x\right)\dot{\varepsilon}_x, \\
\dot{\tau}_{xy} &= G\left(\eta\frac{\pi}{2}\cos\left(2\pi\frac{\varepsilon_x}{E_x}\right) - \frac{E\sigma_x + 3G\eta\frac{\pi}{2}\cos\left(2\pi\frac{\varepsilon_x}{E_x}\right)\tau_{xy}}{E\sigma_x^2 + 9G\tau_{xy}^2}3\tau_{xy}\right)\dot{\varepsilon}_x.
\end{aligned} \tag{4.35}$$

Introducing the trigonometric stress representation (4.5) and the notation (4.8), the incremental relations (4.35) can be presented as follows

$$\frac{\sigma_0}{3G}\dot{\theta} = \frac{\frac{\sqrt{3}\eta}{3}\frac{\pi}{2}\cos\left(2\pi\frac{\varepsilon_x}{E_x}\right)\cos\theta - \sin\theta}{1 + \left(\frac{3G}{E} - 1\right)\sin\theta^2}\dot{\varepsilon}_x \tag{4.36}$$

or

$$d\bar{\varepsilon}_x = \frac{1}{1+m}\frac{1 + m(\sin\theta)^2}{\tan\Phi\frac{\pi}{2}\cos\left(\frac{\bar{\varepsilon_x}}{E_x}\right)\cos\theta - \sin\theta}d\theta, \tag{4.37}$$

where $\bar{\varepsilon}_x = \varepsilon_x/\varepsilon_0$. Eq. (4.37) can be integrated numerically. The elastic unloading condition now is

$$\dot{F} = \sigma_0\left(\cos\theta\dot{\sigma}_x + \sqrt{3}\sin\theta\dot{\tau}_{xy}\right) = \sigma_0\left[\cos\theta + (1+m)\frac{\pi}{2}\frac{\eta}{\sqrt{3}}\cos\left(2\pi\frac{\varepsilon_x}{E_x}\right)\right]\dot{\varepsilon}_x \le 0 \tag{4.38}$$

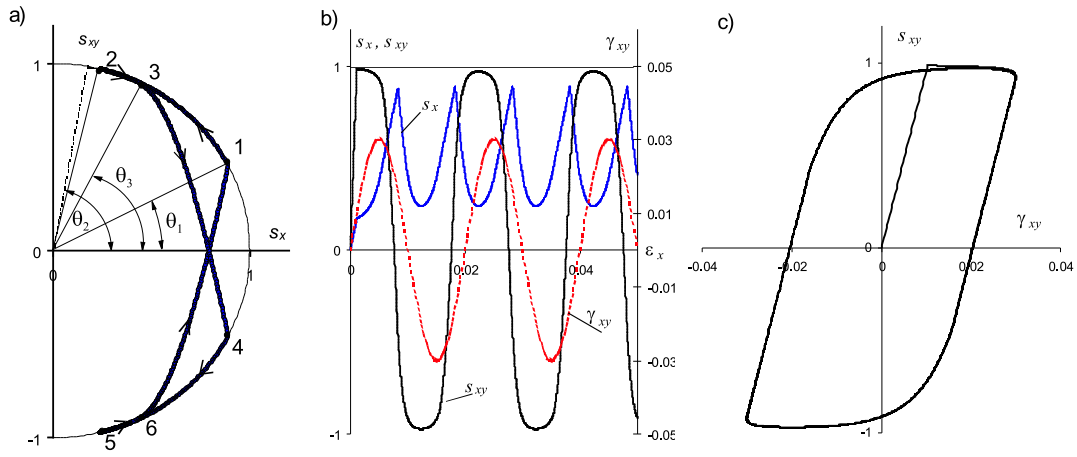

Figure 14. Harmonic shear strain control with maximal axial stress reduction and elasto-plastic response ($\eta = 6$, $\gamma_m/\varepsilon_0 = 4.62$) a/ cyclic stress path, b/ variation of axial and shear stress and shear strain, c/ torsional hysteresis loop.

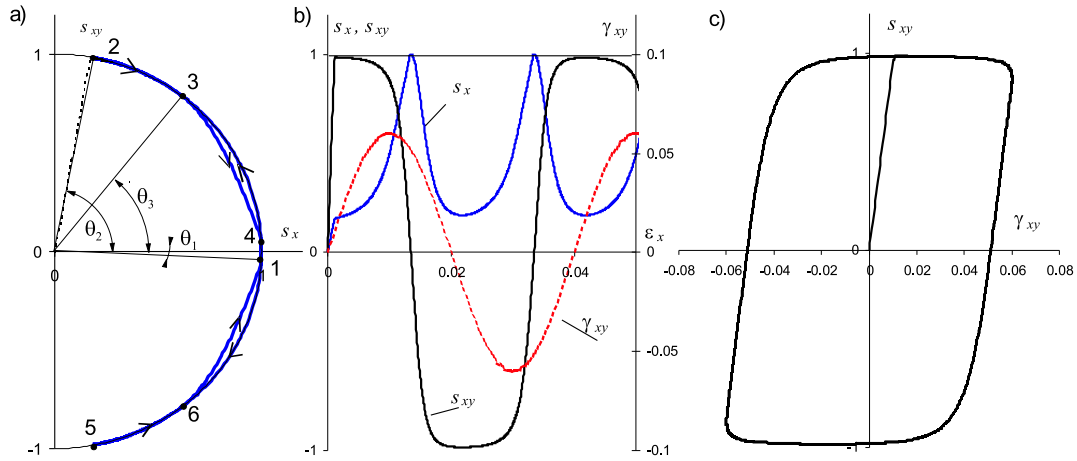

Figure 15. Harmonic shear strain control with no maximal axial stress reduction and elasto-plastic response ($\eta = 6$, $\gamma_m/\varepsilon_0 = 9.24$) a/ cyclic stress path, b/ variation of axial and shear stress and shear strain c/ torsional hysteresis loop.

Introducing the notation

$$\tan\left[\Phi\left(\frac{\bar{\varepsilon_x}}{\bar{E}_x}\right)\right] = \frac{\pi}{2}\frac{\sqrt{3}\eta}{3}\cos\left(2\pi\frac{\bar{\varepsilon_x}}{\bar{E}_x}\right),$$

$$\tan\left[\varphi\left(\frac{\bar{\varepsilon_x}}{\bar{E}_x}\right)\right] = (1+m)\frac{\pi}{2}\frac{\eta}{\sqrt{3}}\cos\left(2\pi\frac{\bar{\varepsilon}_x}{\bar{E}_x}\right) = \frac{\dot{s}^e_{xy}}{\dot{s}^e_x}$$

we obtain from (4.38)

$$\cos(\theta-\varphi) = 0, \quad \theta-\varphi = \pm\frac{\pi}{2},$$

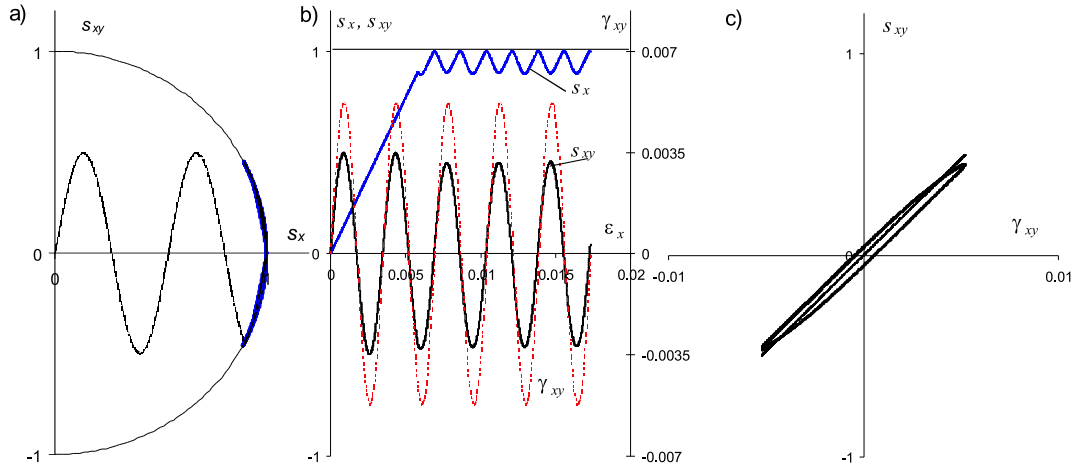

Figure 16. Harmonic shear strain control with no maximal axial stress reduction and plastic response ($\eta = 6$, $\gamma_m/\varepsilon_0 = 0.924$) a/ cyclic stress path, b/ variation of axial and shear stress and shear strain, c/ torsional hysteresis loop.

so the stress trajectory in the s_x, s_{xy}-plane at the instant of unloading is tangential to the yield surface. The elastic stress rates $\dot{s}^e_{xy}$ and $\dot{s}^e_x$ then specify the angle φ.

The reverse point of the axial stress oscillation is specified by the condition $ds_x/d\varepsilon_x = 0$ and then

$$\sin\theta \sin(\Phi - \theta) = 0, \quad \text{so that} \quad \theta = \Phi$$

and the tensile stress reduction occurs when $\Phi < \theta$.

The typical stress paths are presented in Figs 14-16. Similarly as for piecewise linear shear strain control, the response regimes $\mathcal{A}$, $\mathcal{B}$, $\mathcal{C}$ will occur depending on γ_m and η.

Fig. 14 presents the cyclic material response for $\eta = 6$, $\gamma_{m3}/\varepsilon_0 = 4.62$ when the cyclic process is composed of elastic and elastic-plastic portions with the reduction of maximal axial stress (regime $\mathcal{C}$). Fig. 15 presents the cyclic response for $\eta = 6$, $\gamma_{m2}/\varepsilon_0 = 9.24$ when the elastic and elastic-plastic portions occur with no reduction of maximal axial stress (regime $\mathcal{B}$). Fig 16 for $\eta = 6, \gamma_{m1}/\varepsilon_0 = 0.924$ presents the response for small amplitude value and no maximal stress reduction. Fig. 17 presents the cyclic response diagram in the plane $\gamma_m/\varepsilon_0, \eta$. It is seen that the line separating the regimes $\mathcal{A} + \mathcal{B}$ and $\mathcal{C}$ differs essentially from that generated for piecewise linear control. In fact, for instance $\eta = 6$ and increasing γ_m/ε_0, we intersect the domain $\mathcal{C}$ at two points for small and large values of γ_m/ε_0. Thus, there is no reduction of maximal value of s_x for sufficiently small values of $\gamma_m \leq \gamma_{m1}$ and for sufficiently large values $\gamma_m \geq \gamma_{m2}$. For piecewise linear control the separating lines tend to asymptotic values of γ_m/ε_0 and η, cf. Fig. 7. The diagrams shown in Figs 14, 15 and 16 are presented for the values $\gamma_m = \gamma_{m1}$, γ_{m2} and γ_{m3} marked in Fig. 17. It is also demonstrated that the periodic shear strain variation exhibits phase shift with respect to the shear stress variation.

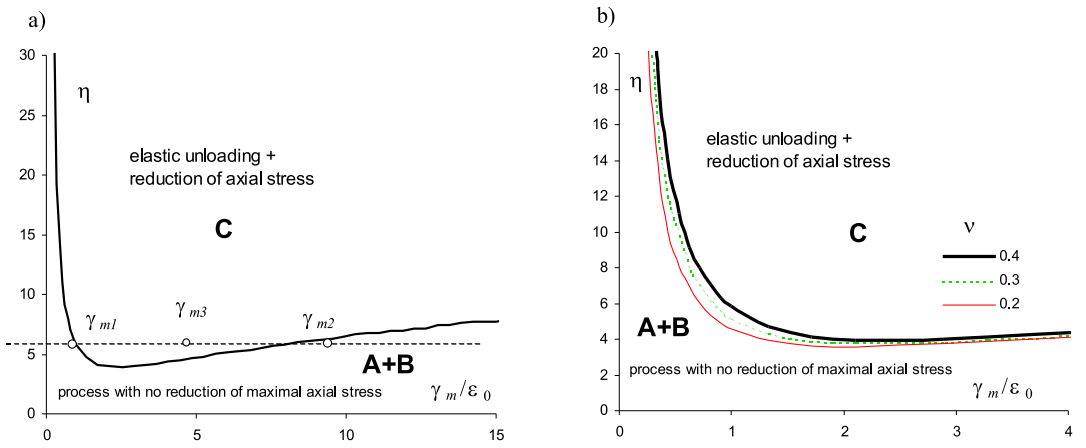

Figure 17. The response diagram in the plane $\gamma_m/\varepsilon_0, \eta$ specifying domains $\mathcal{A}+\mathcal{B}$ and $\mathcal{C}$ of no-reduction and reduction of maximal axial stress a/ diagram for large values of γ_m/ε_0, b/ diagram for small values of γ_m/ε_0

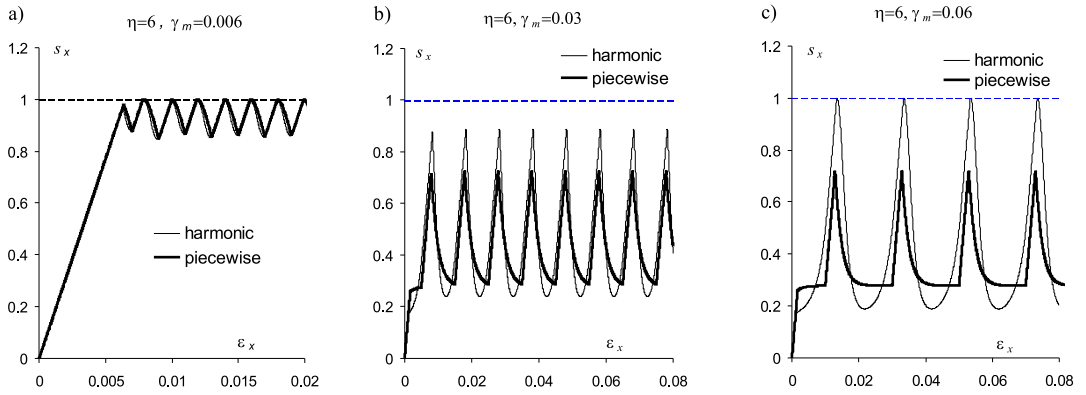

Figure 18. Comparison of the tensile stress paths for piecewise linear and harmonic shear strain controls ($E = 77000$ MPa, $\nu = 0.4$, $\sigma_0 = 500$ MPa, $\eta = 6$), a/ $\gamma_{m1} = 0.006$, b/ $\gamma_{m3} = 0.03$, c/ $\gamma_{m2} = 0.06$. Relative parameter values: $\varepsilon_0 = \sigma_0/E \sim 0.0065$, $\gamma_m/\varepsilon_0 = 0.924; 4.62; 9.24$.

Fig. 18 presents the comparative diagrams of axial stress variation for piecewise linear and harmonic shear strain control for the same values of γ_m and η. It is seen that much bigger axial stress reduction occurs for piecewise-linear control for larger values of γ_m.

5 Approximate cyclic solution for a cylinder

In this section we shall discuss the approximate solution for the steady cyclic state in a cylinder subjected to axial tension or compression combined with cyclic torsion of a specified angular amplitude. We assume that the cylinder is composed of thin walled tubes of varying radii and neglect the radial tube interaction, Fig. 19. Assuming the plane cross section and material incompressibility, the strain

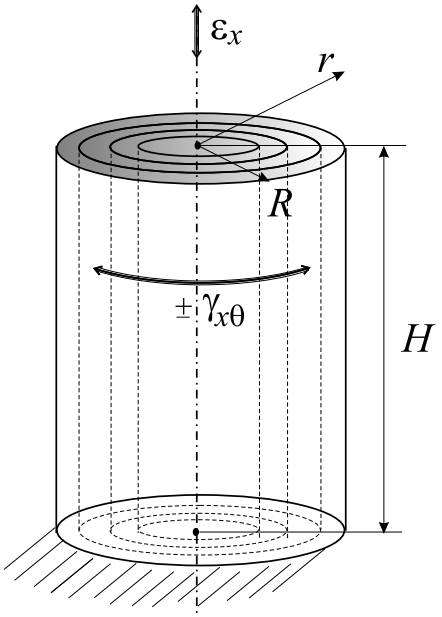

Figure 19. Cylinder geometry

tensor is expressed in the cylindrical coordinate system

$$\varepsilon_x = \varepsilon, \quad \gamma_{x\theta} = \vartheta_r, \quad \varepsilon_r = \varepsilon_\theta = -\frac{1}{2}\varepsilon$$

and the non-vanishing strain rate components are

$$\dot{\varepsilon}_x = \dot{\varepsilon} \quad \dot{\gamma}_{x\theta} = \dot{\vartheta}_r, \quad \dot{\varepsilon}_r = \dot{\varepsilon}_\theta = -\frac{1}{2}\dot{\varepsilon}.$$

Assume the linear variation of shear strain with the radius r and constant tensile strain of each tube, so that

$$\gamma_{x\theta}(r) = \gamma_{x\theta}^R \frac{r}{R}, \quad \varepsilon_x(r) = \varepsilon_x, \quad r = r_0 \exp(\varepsilon_r), \quad \dot{r} = r\dot{\varepsilon},$$

where R is the actual outer radius of the cylinder. The strain rates are

$$\dot{\varepsilon}_x = \dot{\alpha} = const, \quad \dot{\varepsilon}_r = -\frac{1}{2}\dot{\varepsilon} = const, \quad \dot{\gamma}_{x\theta}(r) = \dot{\gamma}_{x\theta}^R \frac{r}{R}$$

Similarly to the case of thin walled tube, two different shear strain programs are considered: piecewise linear and harmonic, so we have

$$\dot{\gamma}_{x\theta}^R = \eta^R \dot{\varepsilon}_x, \quad \text{or} \quad \dot{\gamma}_{x\theta}^R = \eta^R \frac{\pi}{2} \cos\left(2\pi \frac{\varepsilon_x}{E_x}\right) \dot{\varepsilon}_x.$$

5.1 Piecewise linear shear strain control: rigid-plastic model

Assuming the rigid-perfectly plastic model, and using the solution (3.5) for a tube, we can present the stress distribution in the cylinder

$$\sigma_x(\bar{r}) = \frac{\sigma_0}{\sqrt{1+\frac{\eta^2\bar{r}^2}{3}}}, \quad \tau_{x\theta}(\bar{r}) = \pm\frac{\eta}{3}\frac{\sigma_0\bar{r}}{\sqrt{1+\frac{\eta^2\bar{r}^2}{3}}}, \quad \text{where} \quad \bar{r} = \frac{r}{R}. \qquad (5.1)$$

The stress distribution for $\eta = 1$, 3 and 10 is shown in Fig. 20.

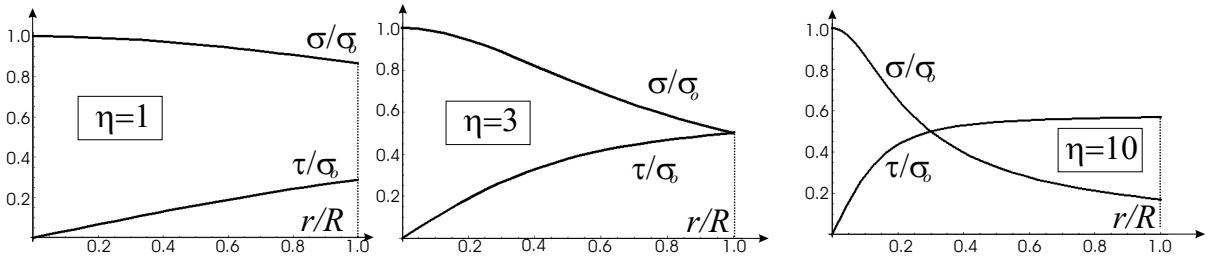

Figure 20. Variation of axial stress and shear stresses in a cylinder for $\eta = 1, 3, 10$

Integrating the axial and shear stresses (5.1) over the actual cross-section of the cylinder, we obtain

$$F = F_0\frac{6}{\eta^2}\left(\sqrt{1+\frac{\eta^2}{3}} - 3\right), \quad M = M_0\frac{\sqrt{3}}{\eta^3}\left((\eta^2-6)\sqrt{1+\frac{\eta^2}{3}} + 6\right),$$

where $F_0 = F(\eta = 0)$ is the axial force in pure tension and $M_0 = M(\eta \to \infty)$ is the twisting moment in pure torsion, so that

$$F_0 = \pi R^2\sigma_0, \quad M_0 = \frac{\sqrt{2}}{3\sqrt{3}}\pi R^3\sigma_0.$$

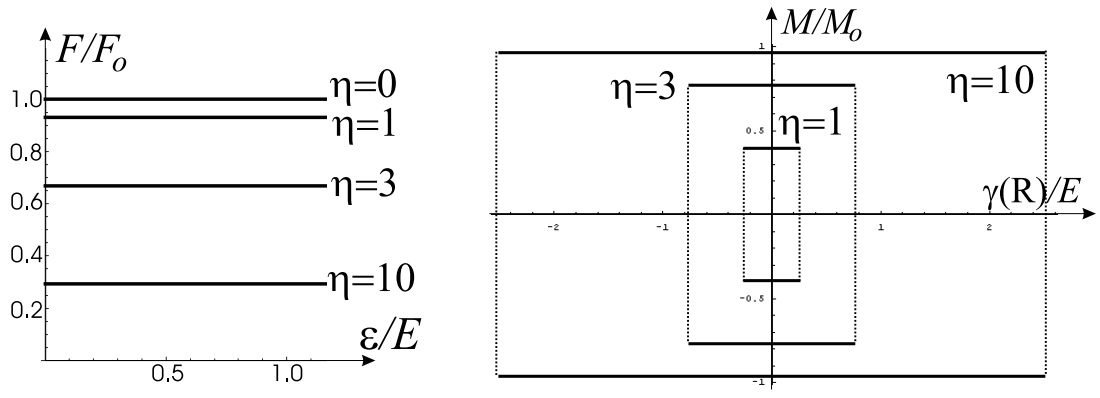

Figure 21. The cross-sectional force and moment variation in the steady cyclic state

Figure 21 presents the evolution of F/F_0 and M/M_0 in the course of cyclic deformation. It is seen that the axial force and the torsional hysteretic loop

depend on the value of parameter η. Figure 22 presents the variation of F/F_0 and M/M_0 with η. It is seen that the axial force decreases and the torsional moment amplitude increases with η.

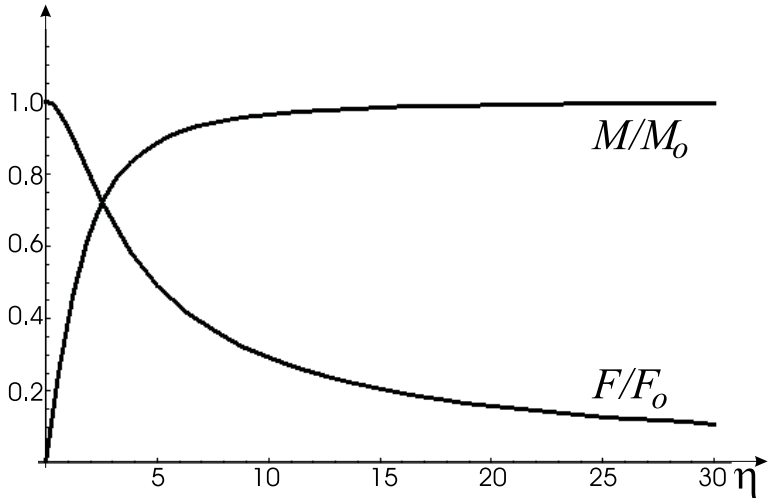

Figure 22. Variation of axial force and twisting moment with the parameter η.

5.2 Harmonic control of shear strain: rigid-plastic model

For the harmonic variation of γ_{xy}, the stress components follow from the solution for a tube, Eq. (3.7), so we have

$$\sigma_x(\bar{r}) = \frac{\sqrt{3}\sigma_0}{\sqrt{3+\eta^2\bar{r}^2\frac{\pi^2}{4}\cos^2(2\pi e)}}, \quad \tau_{x\theta}(\bar{r}) = \pm\frac{\sqrt{3}\sigma_0\bar{r}\eta\frac{\pi}{2}\cos(2\pi e)}{3\sqrt{3+\eta^2\bar{r}^2\frac{\pi^2}{4}\cos^2(2\pi e)}}, \quad (5.2)$$

where $e = \varepsilon_x/E_x$. Figure 23 presents the stress variation within the cylinder for increasing values of e, and the assumed value $\eta = 3$.

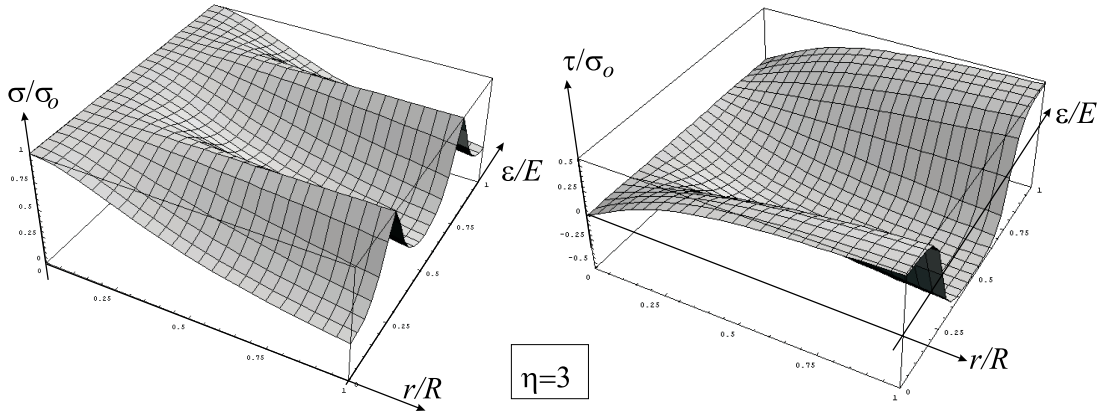

Figure 23. The axial and shear stress distribution in cylinder for $\eta = 3$

The cross sectional axial force and twisting moment are expressed as follows

$$F = F_0 \frac{6}{\eta^2 \frac{\pi^2}{4} \cos^2(2\pi e)} \left(\sqrt{1 + \frac{1}{3}\eta^2 \frac{\pi^2}{4} \cos^2(2\pi e)} - 3 \right),$$

$$M = M_0 \frac{\sqrt{3}}{\eta^3 \frac{\pi^3}{16} \cos^3(2\pi e)} \left((\eta^2 \frac{\pi^2}{4} \cos^2(2\pi e) - 6) \sqrt{1 + \frac{1}{3}\eta^2 \frac{\pi^2}{4} \cos^2(2\pi e)} + 6 \right).$$

Variation of F/F_0 and M/M_0 in the course of steady cyclic deformation is presented in Fig. 24. It is seen that the axial force reaches its maximum equal F_0 and its minimum value strongly depends on η.

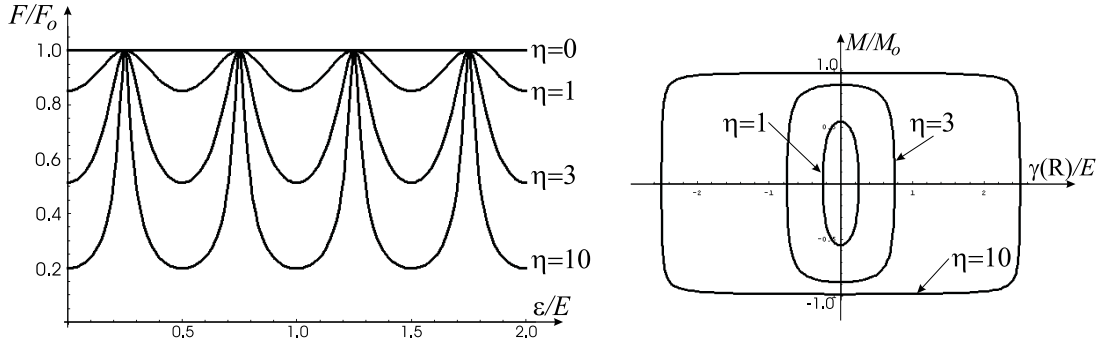

Figure 24. Variation of axial force and twisting moment in the steady cyclic state for different values of η.

5.3 Piecewise linear shear strain control: elastic-plastic model

To simplify the analysis, we shall treat cylinder as a discrete set of thin walled tubes and neglect their radial interaction. The resulting axial force, and torsional moment are obtained by summing up and averaging stress contributions of consecutive tubes. Referring to Fig. 25, it is seen that depending on the value of radius r and sufficiently large values of η, the tubes can correspond to the regimes $\mathcal{A}$, $\mathcal{B}$, and $\mathcal{C}$. Thus in the external cylinder portion $r_2 \leq r \leq R$ the regime $\mathcal{C}$ occurs with elastic unloading and maximal axial stress reduction, cf. Fig. 26, but in the central cylinder portion $0 \leq r \leq r_1$ the regime $\mathcal{A}$ occurs with no elastic unloading during the steady cyclic deformation. In the intermediate portion $r_1 \leq r \leq r_2$ the regime $\mathcal{B}$ occurs with no reduction of maximal tensile stress.

6 Concluding remarks

The present paper provides the analysis of cyclic deformation modes for a tube or cylinder subjected to axial extension or compression with specified rate of displacement, assisted by cyclic torsion of specified strain rate and amplitude. The fundamental process parameters are the ratio of rates of shear and axial

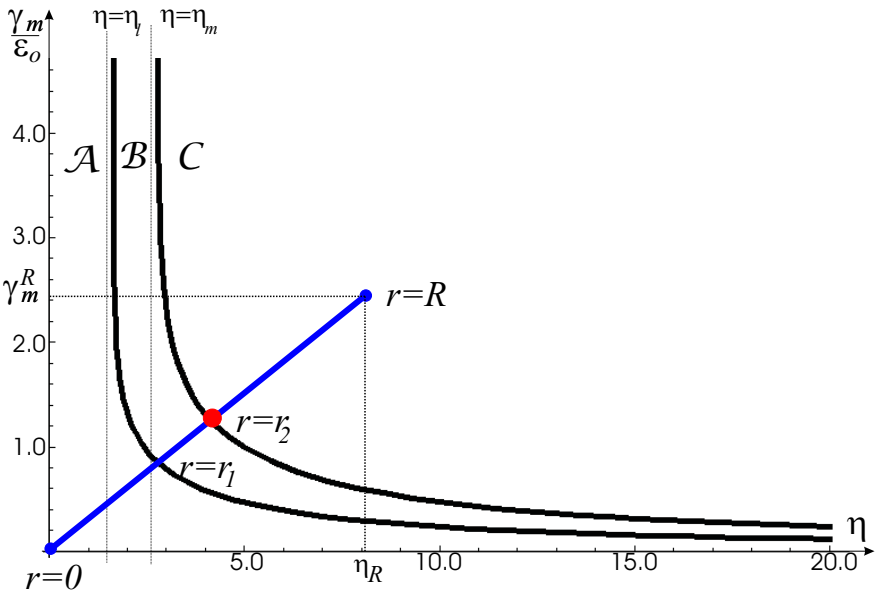

Figure 25. Three different stress regimes within a cylinder subjected to monotonic extension and cyclic torsion

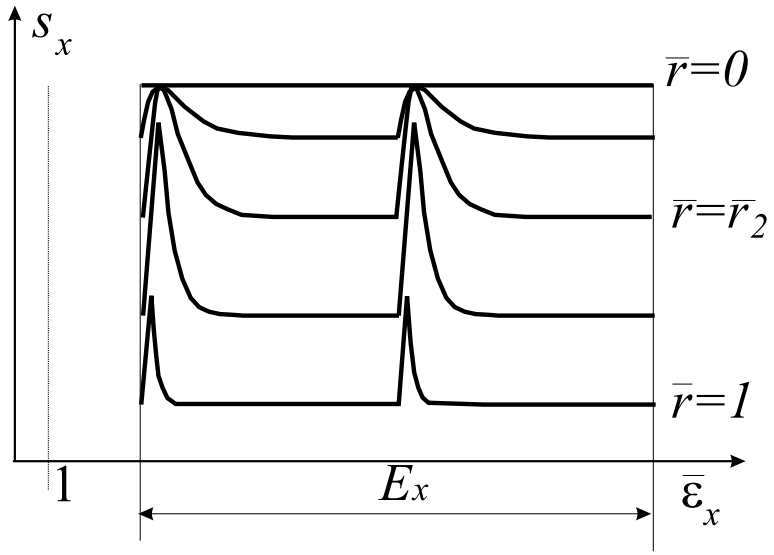

Figure 26. Variation of axial stress within a cylinder in one cycle of twist for varying values of the radius r.

strains η and the shear strain amplitude γ_m . Three different stress regimes are detected and analyzed in detail. The response domains in the plane of process parameters are specified and plotted in the form of diagrams resembling familiar Bree diagrams specifying shake down, alternating plasticity and ratchetting domains for structural elements under load control and a perfectly plastic material response. It is demonstrated that considerable axial force reduction can be attained for sufficiently large values of η and γ_m. However, the plastic energy dissipation in the process is always larger with respect to the pure axial extension or compression for specified total elongation or shortening of the cylinder. The

response for piecewise linear and harmonic shear strain control is illustrated by presenting the cyclic stress path and stress-strain diagrams. The application of material hardening models combined with dynamic recovery effects would provide different results and prediction of reduced energy dissipation. This topic will be the subject of a separate study and confrontation with experimental data. The problem of microstructure evolution in the course of cyclic loading especially, fine grained structure generation will also be analysed. The present paper provides the fundamental clarification of cyclic deformation modes and their dependence on process parameters.

Acknowledgement

The research presented in this paper was supported through National Research Council (KBN) grant No PBZ-KBN-102/TO8/2003.

References

[1] Z.S. Basiński and P.J. Jackson. The instability of the work hardening state (I) - slip in extraneously deformed crystals. *Phys. Stat. Sol.*, 9:805, 1965.

[2] W. Bochniak and A Korbel. Extrusion of CuZn39Pb2 alloy by the KOBO method. *Eng. Trans.*, 47:351–367, 1999.

[3] W. Bochniak and A Korbel. Plastic flow of aluminium extruded, under complex conditions. *Mat. Sci. Technol*, 16:664–674, 2000.

[4] W. Bochniak and A Korbel. KOBO-type forming: forging of metals under complex conditions of the process. *J. Mat. Process. Techn*, 134:120–134, 2003.

[5] F. Grosman and J. Pawlicki. The yield stress in the conditions of combined loadings. *Materiały XII Konferencji KomPlasTech, Informatyka w Technologii Metali (Proceedings of XII Conference KomPlastTech, Informatics in Metal Technology) Ustroń 2005*, pages 253–258, 2005. [in Polish].

[6] P.J. Jackson and Z.S. Basiński. The effect of extraneous deformation on strain hardening in Cu single crystals. *Appl. Phys. Lett.*, 6:148, 1965.

[7] L.F. Coffin Jr. Low-cycle-fatigue: a review. *Appl. Mat. Res.*, 1:129–141, 1962.

[8] L.X. Kong and P.D. Hodgson. Constitutive modeling of extrusion of lead with cyclic torsion. *Mat. Sci. Eng. A*, 276:32, 2000.

[9] L.X. Kong, P.D. Hodgson, and B. Wang. Development of constitutive models for metal forming with cyclic strain softening. *J. Mat. Process. Technol.*, 89-90:44, 1999.

[10] A. Korbel and W. Bochniak. Refinement and control of the metal structure elements by plastic deformation. *Scripta Materialia*, 51:755–759, 2004.

[11] Z. Mróz and P. Rodzik. On multisurface and integral description of anisotropic hardening evolution of metals. *Eur. J. Mech. A/Solids*, 15:1–28, 1996.